HHS Public Access

Author manuscript

Dev Biol. Author manuscript; available in PMC 2024 March 01.

Published in final edited form as:

Dev Biol. 2023 March ; 495: 76–91. doi:10.1016/j.ydbio.2023.01.001.

Identity, Lineage and Fates of a Temporally Distinct Progenitor Population in the Embryonic Olfactory Epithelium

Elizabeth M Paronett[1], **Corey A Bryan**[2], **Thomas M Maynard**[3], **Anthony-S LaMantia**[4]

[1]Department of Pharmacology and Physiology, George Washington University School of Medicine, Washington, DC, 20037, USA.

[2]Laboratory of Developmental Disorders and Genetics, The Fralin Biomedical Research Institute, Virginia Tech-Carilion School of Medicine, Roanoke, VA, USA.

[3]Center for Neurobiology Research, The Fralin Biomedical Research Institute, Virginia Tech-Carilion School of Medicine, Roanoke, VA, USA.

[4]Center for Neurobiology Research, The Fralin Biomedical Research Institute, Virginia Tech-Carilion School of Medicine, Roanoke, VA, USA; Department of Biological Sciences Virginia Tech, Blacksburg, VA, USA.

Abstract

We defined a temporally and transcriptionally divergent precursor cohort in the medial olfactory epithelium (OE) shortly after it differentiates as a distinct tissue at mid-gestation in the mouse. This temporally distinct population of Ascl1+ cells in the dorsomedial OE is segregated from Meis1+/ Pax7+ progenitors in the lateral OE, and does not appear to be generated by Pax7+ lateral OE precursors. The medial Ascl1+ precursors do not yield a substantial number of early-generated ORNs. Instead, they first generate additional proliferative precursors as well as a distinct population of frontonasal mesenchymal cells associated with the nascent olfactory nerve. Parallel to these *in vivo* distinctions, isolated medial versus lateral OE precursors *in vitro* retain distinct proliferative capacities and modes of division that reflect their in *vivo* identities. At later fetal stages, these early dorsomedial Ascl1+ precursors cells generate spatially restricted subsets of ORNs as well as other non-neuronal cell classes. Accordingly, the initial compliment of ORNs and other OE cell types is derived from at least two distinct early precursor populations: lateral Meis1/ Pax7+ precursors that generate primarily early ORNs, and a temporally, spatially, and transcriptionally distinct subset of medial Ascl1+ precursors that initially generate additional OE progenitors and apparent migratory mass cells before yielding a subset of ORNs and likely supporting cell classes.

Graphical Abstract

[1]Corresponding author: anthonysl@vtc.vt.edu.

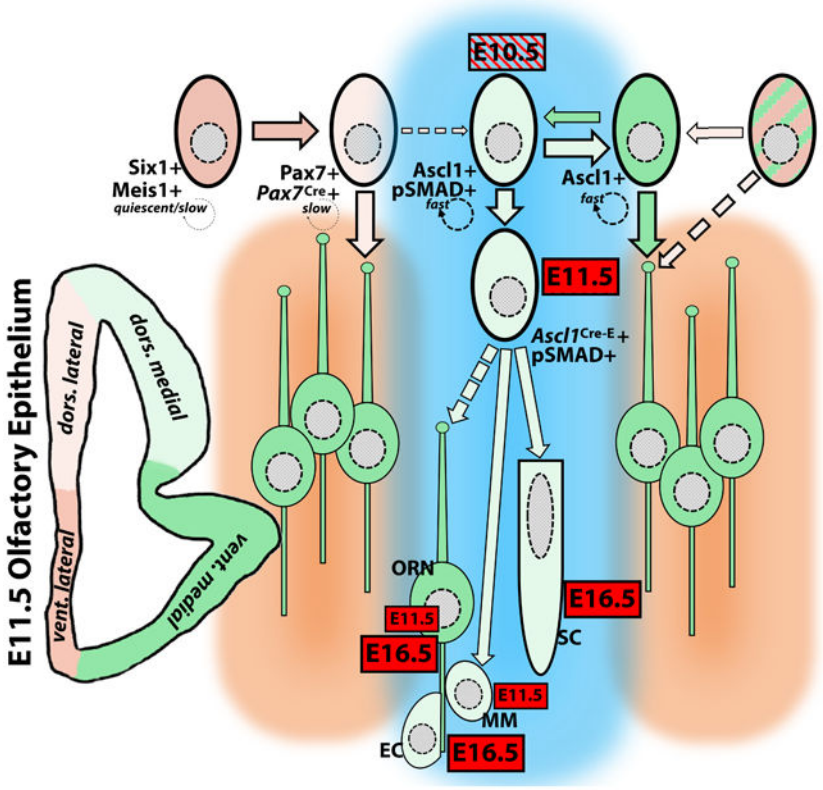

INTRODUCTION

The earliest compliment of olfactory epithelium (OE) precursors generate olfactory receptor neurons (ORNs) (Balmer and LaMantia, 2005; Sokpor et al., 2018) for odor detection, sustentacular cells that ensure OE homeostasis (Brann et al., 2020; Khan et al., 2021; Liang, 2018), ensheathing cells that facilitate ORN axon growth (Franssen et al., 2007; Rigby et al., 2020), and OE stem cells that regenerate these cell classes throughout life (Schwob et al., 2017). Early OE precursors specification may also influence “zonal” odorant receptor expression for ORN functional diversity (Coleman et al., 2019; Monahan and Lomvardas, 2015; Rodriguez, 2013; Sullivan et al., 1995; Zapiec and Mombaerts, 2020). Early OE precursors as well as their adult progeny are currently thought to be a unitary population defined by sequential transcription factor expression (reviewed by Beites et al., 2005; Schwob et al., 2017). Nevertheless, during the initial differentiation of the OE, subsets of OE precursors have distinct proliferative characteristics and responses to local signals (LaMantia et al., 2000; LaMantia et al., 1993; Maier et al., 2010; Shou et al., 2000; Shou et al., 1999; Tucker et al., 2010; Whitesides et al., 1998). We therefore asked whether there are distinctions among early OE precursors, and how such distinctions might influence subsequent OE differentiation.

OE precursor identity and fate has been characterized mostly in the adult where these cells continuously generate ORNs (Child et al., 2018; Coleman et al., 2019; Guo et al., 2010; Iwai et al., 2008; Leung et al., 2007; Liberia et al., 2019). Less attention has been

given to molecular, spatial and temporal distinctions that influence precursor lineage and fate during early OE development. Multiple transcription factors have been localized to OE progenitors, including—but not limited to—Sox2 (Donner et al., 2007; Packard et al., 2016; Panaliappan et al., 2018; Tucker et al., 2010), Six1 (Chen et al., 2009; Ikeda et al., 2007), Meis1 (Toresson et al., 2000a; Tucker et al., 2010), Pax7 (Murdoch et al., 2010; Stoykova and Gruss, 1994), and Ascl1 (Cau et al., 2002; Cau et al., 1997; Gordon et al., 1995; Guillemot et al., 1993). Disrupted ORN genesis due to loss of function mutations in many of the genes that encode these transcription factors has been interpreted to support linear progression of a single class of progenitors that give rise to ORNs and other OE cell types. Nevertheless, additional dimensions of OE precursor diversity may result in regional and molecular distinctions during OE differentiation (Coleman et al., 2019; Yang et al., 2018). Assessing whether early OE precursors are initially subdivided into spatially or temporally diverse cohorts with divergent molecular identities, proliferative characteristics and fate, as is the case in the developing retina (Byerly and Blackshaw, 2009; Shiau et al., 2021), may provide insight into how OE cellular diversity is established.

We asked whether there are distinct populations of early OE precursors with divergent times of origin, molecular identities, proliferative capacities and cell fates among what has previously been assumed to be a fairly homogenous population (Cau et al., 2002; Cau et al., 1997; Murdoch et al., 2010). We found a temporally, molecularly, and proliferatively distinct subset of early-generated Ascl1+ precursors restricted to the dorsomedial OE whose primary immediate progeny are additional precursors as well as cells in the migratory mass rather than ORNs. These Ascl1+ cells subsequently generate spatially segregated ORNs and OE cells types. Thus, as in other cranial sensory organs including the retina (Bassett and Wallace, 2012), inner ear (Fritzsch et al., 2002), and cranial sensory ganglia (Karpinski et al., 2016), the OE likely arises from temporally and molecularly distinct precursor populations with divergent capacities to generate peripheral olfactory sensory neurons and supporting cells.

MATERIALS AND METHODS

Animals:

All animal procedures were reviewed and approved by the George Washington University Institutional Animal Care and Use Committee. *Sox2*^{eGFP} (Ellis et al., 2004), *Pax7*^{Cre} (Keller et al., 2004), *Ascl1*$^{Cre\text{-}E}$ (Battiste et al., 2007), and *Ai9:tdTomato*^{fl} reporter (Madisen et al., 2010) alleles were maintained on a C57Bl6N background. *Sox2* reporter or Cre driver alleles were transmitted paternally and *Ai9*^{fl} reporter alleles maternally. Pregnancies were timed by date of vaginal plug detection after overnight matings as E0.5. Single injections of tamoxifen (10mg/ml; 100µl/dam) were given to pregnant dams carrying *Ascl1*$^{Cre\text{-}E+/-}$:*Ai9* reporter$^{fl/-}$ litters. One subset of dams received an injection of BrdU (50mg/kg body weight) on E11.5, 2 hours or 5 days prior to embryo collection; another received BrdU in their drinking water for 48 hours starting at E11.5, ending on E13.5, prior to collecting fetuses as E16.5. Dams were sacrificed by cervical dislocation. E11.5 and E16.5 embryos/fetuses were fixed by immersion in 4% paraformaldehyde overnight at 4°C, and fetal membranes collected for genotyping.

Tissue processing and immunohistochemical analysis:

Fixed embryos were rinsed in PBS, pH 7.4, transferred to 10%, 20%, then 30% sucrose in 0.1M phosphate buffer (PB) for cryoprotection, embedded in 2.5% agar in 30% PB-sucrose to position them consistently, and flash-frozen in cryoembedding media (OCT) using liquid nitrogen-cooled 2-methyl butane. Blocks were sectioned at 10 μm, serial sections mounted onto slides stored at −20°C before immunostaining. Primary antibodies against tdTomato/red fluorescent protein (RFP; Abcam, rabbit), Pax7 (Developmental Hybridoma Studies Bank, mouse), Meis1 (Abcam, rabbit), Ascl1 (BD Bio, mouse; Chemicon, rabbit), Six1 (Proteintech, rabbit; Atlas, mouse), eGFP (Abcam), pSMAD (Millipore, mouse), BrdU (BD, mouse; Novus, rat), PH3 (Cell Signaling; rabbit), βIII-tubulin (Aves, chicken), NCAM (Millipore, rat), and OMP (Pierce Biotech; chicken) followed by 2° antibodies for single, double or triple label as described previously (Karpinski et al., 2016). Images were collected on a Leica Tiling epifluorescence or Zeiss 710 confocal microscope.

Quantitative analysis of OE cell classes *in vivo*:

We quantified the distribution of OE progenitors and neurons labeled with multiple markers in the E11.5 OE, divided into 10 sectors, each representing 1/10 of the inner OE perimeter (Tucker et al, 2010; Figure 1H, inset). To normalize analyses of multiple individual animals from multiple litters at several locations along the anterior-posterior OE axis, DAPI-labelled cells were also counted in each sector and frequency of each molecular marker was calculated as a percentage, rather than absolute number, of cells in each sector.

Pair Cell Assays:

Sox2^{eGFP} reporter expression was confirmed via fluorescence microscopy in E10.5 embryos and frontonasal processes were micro-dissected (n=4 independent experiments/4 litters). The OE was isolated from multiple embryos/litter, and pooled into medial and lateral samples. These samples were dissociated as described previously (Lehtinen et al., 2011; Shen et al., 2002; Tucker et al., 2010). Equivalent numbers of medial and lateral cells were plated at low density (35 cells/μl; 14 μl total volume/well) on poly-D-lysine coated Terasaki plates and similar numbers of wells were analyzed for each. Cultures were incubated for 21 hours at 37°C with 5% CO_2, fixed and immunolabeled for βIII-tubulin or multiple transcription factor markers (using antibodies summarized above) as well as DAPI to identify nuclei. Pairs of cells in individual wells were identified based upon DAPI labeling as well as eGFP fluorescence based upon apposition of two cells, isolated from any other cells. For each isolated DAPI-labelled pair, expression of eGFP, neural or progenitor markers was visualized and scored.

RESULTS

A distinct population of lateral OE progenitors

We previously defined a population of Meis1+/Pbx1+/low−Sox2+ slowly dividing precursors in the lateral OE in the mid-gestation mouse embryo (Tucker et al., 2010). Pax7+ precursors, which overlap Meis1+ cells (Figure 1A-C), have been identified immunocytochemically and via *Pax7*^{Cre}-mediated recombination in the lateral OE (Murdoch

et al., 2010). These Pax7+ precursors (Figure 1D-F) also generate multiple OE cell types during subsequent OE differentiation (Murdoch et al. 2010). We first asked whether Meis1+ and Pax7+ cells define a single, early OE precursor population. At E10, shortly after the OE has invaginated from the placodal ectoderm, Meis1+ and Pax7+ cells are found throughout the lateral OE (Figure 1A). Lateral Pax7+ and Meis1+ cells overlap in most of the lateral OE at this stage (Figure 1B1-3, asterisks); however, there is a subset of Meis1+/Pax7− dorsolateral OE cells (Figure 1C1-3, asterisks). By E11.5, most of the presumed progeny of Pax7+ cells, labeled via *Pax7*^{Cre}-mediated recombination, remain limited to the lateral OE (Figure 1D, quantified in Figure 1H1). Most *Pax7*^{Cre}+ cells (Figure 1D1) can also be labeled for Pax7+ (Figure 1D2,3). Consistent with limited proliferation and lineage progression for a substantial proportion of Pax7+/Meis1+ and *Pax7*^{Cre}+ cells by E11.5, acutely labeled BrdU+ cell frequency tends to be lower in ventrolateral OE regions where *Pax7*^{Cre}+ cells are most frequent (Figure 1E, see also Figure 1H1,2), and there are few if any *Pax7*^{Cre}+/BrdU+ cells (Figure 1E1, 1H2).

We next asked if there was extensive overlap between Ascl1+ cells, which are thought to be a singular class of rapidly dividing or transit-amplifying OE precursor found throughout the OE (Cau et al., 2000; Cau et al., 1997; Gordon et al., 1995; Murray et al., 2003), and Pax7+ precursor-descended *Pax7*^{Cre}+ cells. At E11.5, most Ascl1+ cells are limited to a dorsomedial domain that is segregated from the region where Pax7+-descended *Pax7*^{Cre}+ cells are found in the lateral OE (Figure 1F). A smaller population of dorsolateral Ascl1+ cells are separated from this dorsomedial population and partially coincide with *Pax7*^{Cre}+ cells (Figure 1F1). In this region we found a small number of Ascl1+/ *Pax7*^{Cre}+/ BrdU+ cells (box, Figure 1F; Figure 1G1-4, asterisks). *Pax7*^{Cre}/Ascl1+ cells are scarce in most sectors, suggesting that Pax7+ descended cells at E11.5 are unlikely to generate substantial numbers of Ascl1+ precursors, especially in the dorsomedial OE. Indeed, few if any Ascl1+ cells in the region of maximal frequency (sectors 6,7) are labeled by *Pax7*^{Cre}-dependent recombination (Figure 1F, see also Figure 1H1,3).

We quantified these impressions of Pax7+-descended (*Pax7*^{Cre}+) versus BrdU+ or Ascl1+ precursor segregation using an unbiased sector analysis to assess regional cell frequencies relatively independently of size, shape and anterior-posterior location in individual developing OEs (Tucker et al., 2010). Each individual OE is divided into 10 geometrically equivalent sectors that correspond to 1/10 of the total length of the inner OE perimeter (Figure 1H, inset). Sectors are labeled counter-clockwise from the nadir of ventral OE (Figure 1H, inset, arrow) so that ventrolateral sector 1 is adjacent to ventromedial sector 10. Thus, sectors 1-4 correspond approximately to the lateral OE, and 5-10 to the medial OE. We assessed frequency of cells labeled by various markers as a percentage of DAPI+ cells in each sector to further minimize variation due to differences in sector areas and cell numbers across the OE. Average cell frequency/sector is presented with error bars (standard error of the mean) to further reflect variation across multiple samples. At boundary regions that coincide, approximately, with sectors with maximal labeled cell frequencies (for example sector 4 and 5; Figure 1D, H) the shape and size of the OE from section to section and animal to animal can result in intermediate frequency values in the “transitional” sectors (for example, sector 5, Figure 1H1). This reflects the unbiased nature of the sector method —it relys only upon OE perimeter measurements that are blind to apparent expression

boundaries (for example dotted lines and arrows, Figure 1D). This variability is reflected in average cell frequencies over multiple sections and animals in transitional sectors like sector 5 (see Figure 1H1); the nature of the unbiased morphometric analysis results in do mean values that cannot fully reflect the far more distinct boundaries seen in individual images.

Pax7^{Cre}+ cell frequency is highest in dorsolateral OE (sectors 3,4; Figure 1H1). There is also a local concentration of *Pax7*^{Cre}+ cells in the ventromedial OE (sector 9; asterisk, Figure 1H1), that mirrors Pax7+ cells seen in this region at E10 (see Figure 1A and inset), which overlaps the ventromedial OE domain from where the vomeronasal organ will form. In contrast, BrdU+ and Ascl1+ cell frequency is maximal in dorsomedial sectors (sectors 6,7; Figure 1H2,3; shaded region). In addition, there is a modest local increase in Ascl1+, but not BrdU+, cell frequency in the ventromedial OE (sector 9; Figure 1H3, asterisk), apparently coincident with the local increase of Pax7^{Cre}+ cells (compare Figures 1D, F, E & H1 asterisks). To confirm the impression that *Pax7*^{Cre}+ cells, Brdu+ cells, and Ascl1+ cells are mostly distinct populations, we quantified the frequency of *Pax7*^{Cre}+/BrdU+ and *Pax7*^{Cre}+/Ascl1+ cells (yellow points/lines, Figure 1H2, 1H3). The frequency of both types of double-labeled cells is low across all OE sectors. Nevertheless, there is a small but detectable population of *Pax7*^{Cre}+/BrdU+ cells in the lateral OE (3-4%, sectors 3, 4; Figure 1H2), and a modest increase of *Pax7*^{Cre}+/Ascl1+ cells in sector 5 of the dorsomedial OE (4% versus 0-1% in most other sectors), perhaps reflecting occasional double-labeled cells seen at the dorsolateral/dorsomedial OE transition (see Figure 1F1, 1G1-4). Despite this modest overlap, *Pax7*^{Cre}+ versus BrdU+ and Ascl1+ OE precursor populations are mostly segregated in the lateral versus dorsomedial OE, respectively.

A distinct population of dorsomedial OE precursors

Previous observations suggest that Ascl1+ cells are distributed fairly continuously throughout the developing OE, and that they divide rapidly as well as asymmetrically to facilitate subsequent OE neurogenesis (Cau et al., 2000; Cau et al., 1997; Guillemot et al., 1993; Murray et al., 2003). Thus, the regionally segregated Ascl1+ cells we identify at E11.5 may be distinct from Ascl1+ cells seen throughout the OE at later embryonic/fetal ages. To further define the identity and immediate fates of these early OE Ascl1+ cells we used a tamoxifen-dependent conditional Cre-recombinase driven by the endogenous *Ascl1* promoter (*Ascl1*$^{Cre\text{-}ERT}$). We gave pregnant dams tamoxifen at E10.5 and then determined the identities and distribution of temporally defined progeny of Ascl1+ cells at E11.5 (Figure 2). E10.5 *Ascl1*$^{Cre\text{-}ERT}$-recombined cells (referred to hereafter as "*Ascl1*$^{Cre\text{-}E}$+ cells") accumulate in the dorsomedial OE at E11.5 (sectors 6,7; Figure 2A, arrows; see also Figure 2H1). This region is distinct from lateral OE regions (sectors 2 through 4) where *Pax7*^{Cre}+ (see Figure 1 and also Figure 2H1). *Ascl1*$^{Cre\text{-}E}$+ cells overlap Ascl1+ cells (Figures 2B, see also Figure 2H2); however, they are not equivalent populations (Figure 2B1-6). In the OE region where *Ascl1*$^{Cre\text{-}E}$+ and Ascl1+ cells reach maximum frequency (sector 7; Figure 2H1,2), Ascl1$^{Cre\text{-}E}$+ cells (19% of DAPI+ cells) are slightly more frequent than Ascl1+ (11%) or Ascl1+/*Ascl1*$^{Cre\text{-}E}$+ cells (6%,). Apparently, *Ascl1*$^{Cre\text{-}E}$+ cells derived from Ascl1+ cells, are segregated in register with additional Ascl1+ cells in the dorsomedial OE.

We further defined the relationship between *Ascl1*$^{Cre\text{-}E}$+ cells and other molecularly distinct OE precursor cell types. Segregation of *Ascl1*$^{Cre\text{-}E}$+ cells from Meis1+ OE precursors (Tucker et al., 2010) is similar to that for *Ascl1*$^{Cre\text{-}E}$+ cells and *Pax7*^{Cre}+ cells (Figure 2C; see also Figure 1, and compare Figure 2H1 with 2H3). We next assessed the relationship between the dorsomedial *Ascl1*$^{Cre\text{-}E}$+ cells and cells likely related to ectodermal placodal precursors that initially give rise to the OE (Horie et al., 2018; Schlosser et al., 2014), most of which express multiple members of the Six family of transcription factors (Chen et al., 2009; Ikeda et al., 2010; Ikeda et al., 2007; Karpinski et al., 2016). Six1+ cells are retained primarily in the E11.5 lateral OE as well as in a medial region that seems to overlap sector 7, where *Ascl1*$^{Cre\text{-}E}$+ cells reach their maximum frequency (Figure 2D; see also Figure 2H4). Some, but not all of *Ascl1*$^{Cre\text{-}E}$+ cells are Six1+ (*inset*, Figure 2D). Thus, although subsets of *Ascl1*$^{Cre\text{-}E}$+ cells share characteristics with additional classes of OE precursors, they appear to be a mostly distinct population.

We next asked if Ascl1Cre+ cells have distinctive proliferative properties. To evaluate whether the *Asc1*$^{Cre\text{-}E}$+ cells are actively proliferating, we assessed their relationship to acutely labeled BrdU+ cells. The frequency of acutely labeled BrdU+ cells is elevated in the dorsomedial regions where Ascl1$^{Cre\text{-}E}$+ cells are seen (sectors 5 - 8, Figure 2E, 2H5; see also Figure 1); however, only a subset of *Ascl1*$^{Cre\text{-}E}$+ cells (approximately one third; see Figure 2H5) are also acutely labeled by BrdU (Figure 2E, 2H5). We also asked whether *Ascl1*$^{Cre\text{-}E}$+ cells coincide with a concentrated population of actively mitotic precursors. Phospho-Histone 3 (PH3)+ presumed actively mitotic cells (von Bohlen und Halbach, 2011), which are not seen in ventral OE (sectors 1 & 10), constitute a small, fairly stable fraction of dorsolateral and dorsomedial OE cells (Figure 2F, 2H6). There is no clear relationship between the mostly apically located PH3+ cells and *Ascl1*$^{Cre\text{-}E}$+ cells. Apparently, although subsets of *Ascl1*$^{Cre\text{-}E}$+ cells are actively proliferating, their proliferative states are neither singular nor uniform.

Inductive signaling molecules are associated with the primary axes of the developing OE: retinoic acid is a primarily lateral signal while Fgf8 acts as a medial signal (LaMantia et al., 2000; LaMantia et al., 1993; Maier et al., 2011; Tucker et al., 2010; Whitesides and LaMantia, 1996). It is not clear, however, whether Bmp4 or other Tgfβ signals, implicated generally in ORN neurogenesis via regulation of Ascl1 at slightly later stages of OE differentiation (Shou et al, 1999; 2000), differentially activate distinct subsets of OE precursors. Bmp4 is localized to the mesenchyme as well as epithelium of the ventral aspect of the olfactory prominences (Bhasin et al., 2003; Rawson et al., 2010). In addition, other Tgfβ family members are available within the OE itself (Gokoffski et al., 2011; Wu et al., 2003). To assess whether Bmps or other Tgfβ signals might differentially influence OE precursor subsets, we analyzed the distribution of phosphorylate (p)SMAD 1/5/8 expressing cells (pSMAD+; Figure 2G), since these pSMADs are key intermediates for Tgfβ signals in neural progenitors (Dincer et al., 2013; Hegarty et al., 2013). pSMAD+ cell frequency is elevated in regions where Ascl1+ and *Ascl1*$^{Cre\text{-}E}$+ cells are also most frequent (Figure 2G, 2G1-3, 2H7). This increase of pSMAD1/5/8+ cells in the medial versus lateral OE suggest that medial OE cells, including those descended from Ascl1+ precursors may be differentially responsive to locally available frontonasal Bmps or other Tgfβ signals.

Early generated *Ascl1*$^{Cre\text{-}E}$+ cells and initial differentiated OE neurons

We next asked whether E11.5 medial *Ascl1*$^{Cre\text{-}E}$+ precursors generate nascent ORNs recognized by expression of βIII-tubulin, a selective marker for early generated ORNS (Roskams et al., 1998). Presumed ORNs, identified based upon cytology as well as βIII-tubulin expression, are seen occasionally in the domain where *Ascl1*$^{Cre\text{-}E}$+ cells are found. Their frequency, however, appears lower in this region than flanking dorsomedial, dorsolateral, and mid-ventrolateral regions (Figure 3A1-2). In addition, βIII-tubulin+ presumed ORNs are either rare or excluded from ventromedial and ventrolateral OE regions where Pax7+ precursors are concentrated (see also Figure 1). Many of βIII-tubulin+ cells have apically oriented dendrites and dendritic knobs further reinforcing their presumed ORN identity (Figure 3B1-3, Figure3C, arrows). βIII-tubulin+ presumed ORNs appear more frequently in OE regions beyond the *Ascl1*$^{Cre\text{-}E}$+ domain (Figure 3A1-2, C). A few βIII-tubulin+ cells are *Ascl1*$^{Cre\text{-}E}$+ and appear to be ORNs; however, most *Ascl1*$^{Cre\text{-}E}$+ cells are not βIII-tubulin+ (Figure 3A1, B1-3). The relationship between the OE region where *Ascl1*$^{Cre\text{-}E}$+ cells are most frequent, the complimentary region where Pax7+ and *Pax7*^{Cre} cells are primarily found, and βIII-tubulin+ presumed ORNs suggests that there may be at least two regionally and molecularly distinct precursor zones in the OE. One zone likely consists of Pax7+/Meis1+ derived precursors that are more likely to generate early ORNs, while the other descends directly from Ascl1+ OE cells and is less likely to generate early ORNs.

We next assessed the distribution of NCAM+ presumed ORNs, which are thought to be actively extending an axon into the ON (Miragall et al., 1989; Yamashita et al., 1998). In individual sections through the E11.5 OE from multiple embryos, NCAM+ cells appear to be excluded or rare in the domain where *Ascl1*$^{Cre\text{-}E}$+ cells are concentrated (Figure 3D1,2, and see below). The cytology of NCAM+ cells in the dorsolateral, ventromedial and dorsomedial OE (Figure 3E) suggests that many are ORNs. In the regions flanking the dorsomedial *Ascl1*$^{Cre\text{-}E}$+ domain, apparent NCAM+ ORNs with apical dendrites and dendritic knobs can be seen (Figure 3F1-3). These presumed ORNs, however, have apical and basal NCAM+ epithelial cells as neighbors. We did not find NCAM+ presumed ORNs within the *Ascl1*$^{Cre\text{-}E}$+ domain (Figure 3D1,2 and supplemental Figure). Instead, we see occasional NCAM+/*Ascl1*$^{Cre\text{-}E}$+ epithelial cells at apical and mid-levels of the OE (Figure 3G1-3). Apparently, the neurogenic capacity of the medial *Ascl1*$^{Cre\text{-}E}$+ cells, and presumably Ascl1+ precursors from which they likely descend, is distinct from that of dorsolateral/dorsomedial/ventromedial Pax7+/Meis1+ precursors.

We quantified the distribution of *Ascl1*$^{Cre\text{-}E}$+, NCAM+ and *Ascl1*$^{Cre\text{-}E}$+/NCAM+ double-labeled OE cells in a series of sections labeled for both markers across multiple OEs at varying anterior-posterior (A-P) levels to further assess the spatial relationship between these populations (Figures 3H,I). When the distribution of *Ascl1*$^{Cre\text{-}E}$+ and NCAM+ cells is expressed as a percentage of all cells (DAPI+; see Methods) in each sector (Figure 3H), the two populations are not in register, and the double-labeled population is consistently below 1%. Variation in OE size and differences in shape along the A-P axis over multiple animals makes it difficult to quantify precisely the apparent absolute exclusion seen in individual sections (see Supplemental Figure 1). In some sections there appear to be appreciable

numbers of NCAM+ cells in the dorsolateral OE (Figure 3A1,2 and D1,2, see also Supplemental Figure 1); for example, in the region of the dorsolateral OE corresponding to the morphometrically defined sector 4. Mean values tend to either diminish or enhance apparent boundaries seen in individual sections, and the average frequency of NCAM+ cells in sector 4 is fairly low across the entire sample (Figure 3H, I). These data reflect relationships between distribution of distinct cell classes (e.g. Ascl1Cre-E+ versus NCAM +) and overall probabilities of detecting each class in a particular OE region. The sectors cannot be interpreted as absolute divisions. Nevertheless, peak *Ascl1*$^{Cre\text{-}E}$+ cells frequency is seen in sector 7 versus NCAM+ cells in sector 9 with a secondary NCAM peak in flanking sector 6; Figure 3H). Consistent with a bias toward segregation of the two populations, NCAM+ cell frequency is substantially lower in sector 7 where *Ascl1*$^{Cre\text{-}E}$+ cells reach highest frequency. An analysis of absolute numbers, rather than proportions, of *Ascl1*$^{Cre\text{-}E}$ and NCAM+ cells in each sector (Figure 3I) yields a similar distribution. The absolute numbers of NCAM+ cells in transitional sectors like sector 8 (more dorsomedial, where fewer NCAM+ cells are seen) versus sector 9 (more ventromedial, where more NCAM+ cells are seen) reinforces the impression that there is a distinction between the distribution of the *Ascl1*$^{Cre\text{-}E}$+ apparent precursors and NCAM+ presumed early generated ORNs in the E11.5 OE.

OE precursor diversity and cellular diversity in the frontonasal mesenchyme

Previous observations suggest that cells from the differentiating OE migrate into the frontonasal mesenchyme (fnm) during early olfactory pathway formation (LaMantia et al., 2000; Miller et al., 2010; Rawson et al., 2010). There is no evidence of Ascl1 expression in the fnm in mid-gestation mice (Guillemot and Joyner, 1993; Parras et al., 2002; Toresson et al., 2000b; Ware et al., 2016). Thus, we asked whether *Ascl1*$^{Cre\text{-}E}$+ cells, likely derived from Ascl1+ OE precursors, contribute to the fnm. We found a small population of *Ascl1*$^{Cre\text{-}E}$+ cells in the E11.5 fnm, distal to the OE, in an aggregate (Figure 4A, and *inset*) that resembles the migratory mass—cells from the OE that interact with early growing ORN axons (Miller et al., 2010; Miragall and Dermietzel, 1992; Miragall et al., 1989; Morse et al., 1998; Schwarting et al., 2007; Whitesides and LaMantia, 1996). Two early ORN markers, βIII-tubulin and NCAM, are also diagnostic markers for migratory mass cells (Miller et al., 2010; Miragall and Dermietzel, 1992; Miragall et al., 1989). Thus, we assessed the coincidence of βIII-tubulin, NCAM and *Ascl1*^{Cre}-E+ cells in the E11.5 fnm. βIII-tubulin+ cells and processes are associated with *Ascl1*$^{Cre\text{-}E}$+ fnm cells (Figure 4B-G). *Ascl1*$^{Cre\text{-}E}$ labeling is limited to perinuclear cytoplasm surrounding fnm cell nuclei (Figure 4A, C1, D1, E1, F1, G1, I1, J1). βIII-tubulin labels small ORN axon fascicles as well as apparent single axons (Figure 4C2, D2, E2, F2, and G2). In some cases, βIII-tubulin+ processes may belong to βIII-tubulin+/*Ascl1*$^{Cre\text{-}E}$+ fnm cells (Figure 4E2, F2). *Ascl1*$^{Cre\text{-}E}$+ fnm cells also coincide with NCAM+ cells and processes (Figure 4H and *inset*; Figure 4I,J). As for βIII-tubulin, NCAM labels single axons as well as small fascicles that do not fully overlap *Ascl1*$^{Cre\text{-}E}$+ fnm cells (Figure 4I1-3, J1-3). The near absence of NCAM+/*Ascl1*$^{Cre\text{-}E}$+ presumed ORNs in the OE (see Figure 3 and supplemental Figure) makes it unlikely that the *Ascl1*$^{Cre\text{-}E}$+ cells, even those that are also NCAM+ (Figure 4J1-3), coincide with axons from *Ascl1*$^{Cre\text{-}E}$+ presumed ORNs.

The accumulation of *Ascl1*$^{Cre\text{-}E}$+ fnm cells with multiple characteristics of migratory mass cells suggest that Ascl1+ OE precursors contribute to the frontonasal mesenchyme (fnm), further defining the fnm as a mosaic of cells with distinct molecular identities, derivations, and signaling capacities (reviewed by LaMantia, 2020). At E11.5, most medial as well as some dorsolateral fnm cells express Six1 (Figure 5A), while most lateral as well as some dorsomedial fnm cells express Pax7 (Figure 5B). Migratory mass cells, including *Ascl1*$^{Cre\text{-}E}$+ cells, express neither Six1 nor Pax7 (Figure 5A, B, *insets*). Dorsal medial fnm cells, including those adjacent to the OE region where Ascl1+ cells are found, do not express Ascl1 (Figure 5C) express Six1 (Figure5D, see also Figure 5B *inset*). *Ascl1*$^{Cre\text{-}E}$+ cells associated with the migratory mass are distinct from both Six1+ cells (Figure 5E1-2) as well as the small number of *Pax7*^{Cre}+ cells found in the medial OE (Figure 5F1,2). NCAM+ cells as well as apparent single or small fascicles of NCAM+ axons can be seen intercalated among *Pax7*^{Cre}+ fnm cells at the boundary of the lateral and medial fnm (Figure 5F1,2). We assessed quantitatively the registration of NCAM+ axons and cells with *Pax7*^{Cre}+ fnm cells using a Pearson correlation analysis of individual pixels labeled for each marker on the original images without processing to enhance brightness and contrast or diminish background. We found a mean correlation of 0.095 ± 0.08 (Pearson correlation coefficient; n=4), suggesting that NCAM+ ORN axons and *Pax7*^{Cre}+ cells are independent entities. In contrast, there is substantial, but not absolute, registration of NCAM+ and *Ascl1*$^{Cre\text{-}E}$+ fnm cells and processes (Figure 5D1-2, 5E1-3). When the coincidence of *Ascl1*$^{Cre\text{-}E}$+ and NCAM+ cells and processes is compared statistically based upon frequency of pixel superimposition as above, the mean correlation, 0.806 ± 0.03 (n=5) is substantial, suggesting a robust relationship between the two. Apparently, Ascl1+ OE precursors contribute to the fnm, in parallel with subpopulations of neural crest derived cells (Anchan et al., 1997; Barraud et al., 2010; Forni et al., 2011; Osumi-Yamashita et al., 1994).

We next asked whether *Ascl1*$^{Cre\text{-}E}$+ fnm cells are distinguished by additional characteristics associated with cells in the early migratory mass or with *Ascl1*$^{Cre\text{-}E}$+ cells in the dorsomedial OE at E11.5. The initial cells that populate the migratory mass are thought to proliferate little, if at all (Miller et al., 2010; Palaniappan et al., 2019). Thus, we assessed the proliferative state of *Ascl1*$^{Cre\text{-}E}$+ cells in the medial dorsal fnm based upon acute BrdU labeling. The limited population of *Ascl1*$^{Cre\text{-}E}$+ cells in the medial dorsal fnm is not labeled by acute BrdU exposure for 2 hours prior to collecting embryos on E11.5, in contrast with robust BrdU labeling of cells in the OE as well as subsets of cells in the lateral and medial fnm (Figure 5G and *inset*). In addition, we found a spatially limited subset of pSMAD+ cells in the fnm that coincide with *Ascl1*$^{Cre\text{-}E}$+ cells and processes (Figure 5H). This restricted fnm population includes pSMAD+/*Ascl1*$^{Cre\text{-}E}$+ cells, as well as cells labeled for one of the two markers only (Figure 5I1,2, 5J1-3). *Ascl1*$^{Cre\text{-}E}$ labeling is seen in the peri-nuclear cytoplasm and proximal processes of presumed migratory mass cells in which the nucleus is pSMAD+(Figure 5K1-3). When one compares the marker profile of known migratory mass cells, Ascl1Cre-E+ cells in the fnm, and the majority of fnm cells (Figure 5L), it is apparent that *Ascl1*$^{Cre\text{-}E}$+ fnm cells and migratory mass cells are likely an overlapping sub-population of medial fnm cells associated with the nascent ON.

Identity and mode of division of distinct E11.5 OE progenitor lineages

The temporal and spatial diversity of early OE precursors and their progeny suggests that medial versus lateral OE precursors differ in their molecular or proliferative characteristics. To further assess such differences, we used a pair cell assay (Shen et al, 2002; Tucker et al, 2010; Lehtinen et al, 2011; Karpinski et al, 2021) to distinguish molecular identities, modes of division and fates of isolated E11.5 medial versus lateral OE precursors. A *Sox2*^{eGFP} reporter expressed throughout the developing OE but not in the fnm (Ellis et al, 2004; Tucker et al, 2010) identifies neural precursors from the dissected E11.5 medial and lateral OE (Figure 6A). Subsets of *Sox2*^{eGFP}+ isolate precursor pairs from the medial as well as lateral OE express Six1 (Figure 6B), Pax7 (Figure 6C), Ascl1 (Figure 6D), and βIII-tubulin (Figure 6E). Thus, these OE precursors retain several aspects of their OE identity, including the capacity to generate presumed neurons.

We analyzed labeled pairs in two ways: first, as a proportion of *all pairs medial or lateral* in which at least one cell is *Sox2*^{eGFP}+ (a small number of pairs are *Sox2*^{eGFP}−, most likely from fnm not fully dissected from the OE samples). Medial OE precursors appear more proliferative based on recovery of more *Sox2*^{eGFP}+ medial versus lateral *Sox2*^{eGFP}+ pairs after plating equivalent dissociated cell numbers (medial=1589 total *Sox2*^{eGFP} pairs; lateral=829 *Sox2*^{eGFP}+ pairs; n=4 independent experiments). The percentage of all *Sox2*^{eGFP} + medial versus lateral pairs labeled for at least one of markers analyzed *in vivo*, however, did not differ significantly (Figure 6F1). Next, we analyzed medial vs. lateral Six1+, Pax7+, Ascl1+ and βIII-tubulin+ pairs as a proportion of *Sox2*^{eGFP}+ medial versus lateral pairs, respectively. Six1+ medial pairs were proportionately more frequent (17% medial, 13% lateral; p≤0.04; Fisher Exact; Figure 6F2) and Pax7+ lateral pairs were more frequent (4% medial, 14% lateral; p≤0.00001; Fisher Exact; Figure 6F2). In contrast, Ascl1+ and βIII-tubulin+ pairs, presumably yielded by precursors with a neurogenic bias do not differ in frequency (Figure 6F2). We next analyzed Six1+, Pax7+, Ascl1+ or βIII-tubulin+ *pairs as a proportion of all pairs*, medial and lateral, that express at least one marker, thus excluding *Sox2*^{eGFP}+ pairs with unknown second order molecular identity. Pax7+ lateral pairs are more frequent (13% medial, 38% lateral; p≤0.00001; Fisher Exact; Figure 6F3), as are Ascl1+ medial pairs (17% medial, 10% lateral; p≤0.03; Fisher Exact; Figure 6F3). Together, these results are consistent with enhanced presence of Pax7+ precursors and progeny in the lateral OE and elevated frequency of Ascl1+ precursors and their progeny in the medial OE.

Subclasses of OE precursors, despite an overall equivalence of medial versus lateral symmetric and asymmetric divisions, are also biased toward symmetric versus asymmetric division. Six1+ medial as well as Six1+ lateral precursors divide symmetrically significantly more frequently (64% vs. 36 % medial /63% vs. 37% lateral symm. vs. asym.; p≤0.0001, medial; ≤0.03, lateral pirs; Fisher Exact; Figure 6G1). Pax7+ medial precursors divide asymmetrically significantly more frequently (67% asymmetric; p≤0.03; Fisher Exact; Figure 6G2). Medial and lateral Ascl1+ precursors divide symmetrically or asymmetrically with approximately equivalent frequency (Figure 6G3). The neurogenic yield (βIII-tubulin+) from *Sox2*^{eGFP}+ medial and lateral asymmetric and symmetric divisions is equivalent

(Figure 6G4). Thus, OE precursor proliferation and modes of division reflect medial versus lateral OE position and molecular identity.

E11.5 *Ascl1*$^{Cre\text{-}E}$ + OE precursors and their E16.5 neuronal and non-neuronal progeny

We next asked whether the E10.5-recombined (E10.5-R) *Ascl1*$^{Cre\text{-}E}$ + temporal/lineage cohort gives rise to spatially-restricted differentiated OE cell classes at E16.5, as the OE grows and acquires a more mature turbinate morphology (Figure 7A1-4). At E16.5, E10.5-R *Ascl1*$^{Cre\text{-}E}$+ cells are found primarily in the more OE anterior portion. From the most anterior (Figure 7A1,2) to mid-anterior levels (Figure 7A3,4), E10.5-R *Ascl1*$^{Cre\text{-}E}$+ cells are distributed discontinuously (Figure 7A1, *inset*), and they are most prominent in the ventral mid-anterior E16.5 OE (Figure 7A2,3). Posterior to this region, a patchy ventral distribution returns in medial turbinates (Figure 7A4). The cytology of E10.5-R *Ascl1*$^{Cre\text{-}E}$+- derived cells varies in the E16.5 OE (*insets*; Figure 7B-D). Some have morphological characteristics of ORNs, others resemble sustentacular cells, and far less frequently, basal cells (Figure 7B,C), based upon OE location and cytological features (Salazar et al., 2019; Schwob, 2002). There are few, if any, E10.5-R *Ascl1*$^{Cre\text{-}E}$+ cells in the respiratory epithelium, identified based upon its distinct cytology (Figure 7D). In addition, there are individual E10.5-R *Ascl1*$^{Cre\text{-}E}$+ cells in lamina propria, adjacent to the OE, as well as subsets of *Ascl1*$^{Cre\text{-}E}$+ processes (Figure 7C, asterisks; Figure 7E, arrowheads). To assess retention of proliferative capacity versus neurogenesis of E10.5-R *Ascl1*$^{Cre\text{-}E}$+ cells, we gave dams carrying E10.5-R *Ascl1*$^{Cre\text{-}E}$ litters BrdU in their drinking water for 48 hours starting at E11.5 and assessed heavily labeled OE cells in their E16.5 fetuses. If a substantial number of E10.5-R *Ascl1*$^{Cre\text{-}E}$+ cells generate ORNs between E11.5 and E13.5, then E16.5 *Ascl1*$^{Cre\text{-}E}$+/BrdU+ ORNs should be fairly numerous. If, however, E10.5-R *Ascl1*$^{Cre\text{-}E}$+ cells divide more frequently before generating post-mitotic ORNs, few *Ascl1*$^{Cre\text{-}E}$+ E16.5 ORNs would be BrdU+ due to serial dilution of the label as the Ascl1+ progenitors divide. Our data favors the latter possibility; we found very few E10.5-R *Ascl1*$^{Cre\text{-}E}$+ cells in the E16.5 OE are BrdU+ (Figure 7F1-3). This is consistent with the suggestion that E10.5-R *Ascl1*$^{Cre\text{-}E}$+ precursors generate additional precursors (see also Figure 2E and Figure 2H5) after they emerge as a distinct population by E11.5 and for the next two days after, and subsequently generate a subset of ORNs and additional apparently differentiated OE cell classes.

To assess neuronal versus non-neuronal cells within the E10.5-R *Ascl1*$^{Cre\text{-}E}$+ cohort, we double-labeled E10.5-R *Ascl1*$^{Cre\text{-}E}$+ cells at E16.5 for NCAM and OMP. NCAM distinguishes actively differentiating ORNs, while OMP is likely associated with ORNs whose axons have reached the olfactory bulb (Graziadei et al., 1980). NCAM+ ORN apical dendrites and knobs are intercalated among E10.5-R *Ascl1*$^{Cre\text{-}E}$+/NCAM− cells with dome shaped apical domains and apically positioned nuclei (Figure 7G, *inset*). We did not detect E10.5 R *Ascl1*$^{Cre\text{-}E}$+/NCAM+ ORNs at E16.5; however, occasional E10.5 R *Ascl1*$^{Cre\text{-}E}$+/NCAM− cells are found among the more substantial population of NCAM+ presumed ORNs (Figure 7H). There is partial registration of NCAM+ axon fascicles and *Ascl1*$^{Cre\text{-}E}$+ cells and processes in the lamina propria (Figure 7I1-3, arrowheads). These fascicles reflect the confluence of smaller NCAM+ fascicles or single NCAM+ axons that are not *Ascl1*$^{Cre\text{-}E}$+ (Figure 7I1-3, arrows). OMP+ cells appear less frequently in the E16.5

OE (Figure 6J), and *Ascl1*$^{Cre\text{-}E}$+/OMP+ presumed ORNs represent a small subset of OMP+ ORNs (Figure 7J1, see also 7L, O, and P). Adjacent to the OMP+ and OMP+/*Ascl1*$^{Cre\text{-}E}$+ presumed ORNS are additional *Ascl1*$^{Cre\text{-}E}$+/OMP− cells with apical domes and apical nuclei (Figure7K-Q). Subsets of OMP+/*Ascl1*$^{Cre\text{-}E}$- distal dendrites and dendritic knobs are segregated from E10.5-R *Ascl1*$^{Cre\text{-}E}$+/OMP− cells with apical domes and apical nuclei (Figure 7P1-3, Q1,2, arrowheads). Finally, we assessed the relationship between E10.5-R *Ascl1*$^{Cre\text{-}E}$+ and OMP+ cells or processes in the lamina propria (Figure 7O1-3). We found no OMP+ cells in the lamina propria, and there is less overlap of OMP+ fascicles and *Ascl1*$^{Cre\text{-}E}$+ cells than that for NCAM+ cells and processes (compare Figure 7R, R1-2 with 7H, 7I1-3). Instead, subsets of *Ascl1*$^{Cre\text{-}E}$+ cells are occasionally adjacent to OMP+ axon fascicles (Figure 7R, R1,2). This analysis of OE neuronal markers, cytology, and cell position distinguishes three classes of E10.5-R *Ascl1*$^{Cre\text{-}E}$ + cells at E16.5 (Figure 7S): 1) NCAM+ or OMP+ cells with apical dendrites and dendritic knobs in the mid-OE that are presumed ORNs. 2) NCAM− and OMP− cells with apical domes and apical nuclei that are presumed sustentacular cells. 3) NCAM+, OMP− cells in the lamina propria adjacent to NCAM+ as well as OMP+ axon fascicles—key properties of olfactory ensheathing cells.

A distinct population of E10.5 Ascl1 precursor-derived cells in the lamina propria

E16.5, E10.5-R *Ascl1*$^{Cre\text{-}E}$+ cells in the lamina propria are closely associated with subsets of NCAM+ and OMP axons. These cells are seen in the lamina propria proximal to *Ascl1*$^{Cre\text{-}E}$+ cells in the E16.5 OE (see Figure 7), as well as adjacent to the VNO, where they surround fascicles of NCAM+ axons (Figure 8A,B and *inset*). This population of *Ascl1*$^{Cre\text{-}E}$+ cells is in an identical position to cells identified previously as olfactory ensheathing cells (Barraud et al., 2010; Forni et al., 2011; Perera et al., 2020). NCAM+ axon fascicles coincide with chains and aggregates of *Ascl1*$^{Cre\text{-}E}$+ cells in the lamina propria as they extend toward larger fascicles (Figure 8C, see also Figure 8a *inset*). In cross section, apparent processes of *Ascl1*$^{Cre\text{-}E}$+ cells define septa that divide sub-fascicles of NCAM+ ORN axons (Figure 8D, E1-3). Discrete bundles of NCAM+ ORN axons and *Ascl1*$^{Cre\text{-}E}$+ cells and processes are often distinct (Figure 8F1-5). While some NCAM+ axon fascicles are apparently fully invested by *Ascl1*$^{Cre\text{-}E}$+ cells and processes, other NCAM+ fascicles and *Ascl1*$^{Cre\text{-}E}$+ cells and processes are not in complete registration (Figure 8F2,3, arrows), and *Ascl1*$^{Cre\text{-}E}$+ cell processes extend beyond individual axon bundles (Figure 8F4,5). The relationship between E10.5-R *Ascl1*$^{Cre\text{-}E}$+ cells and OMP+ axons at E16.5 is distinct from that with NCAM+ axons (Figure 8G-J). *Ascl1*$^{Cre\text{-}E}$+ cells and processes are not OMP+ (Figure 8G,H). Instead, these cells form capsules that envelop multiple fascicles that include OMP+ axon as they exit the OE. OMP+ ORN axons appear to be intercalated with presumed OMP− axons within single fascicles (Figure 8H; arrowheads). Some OMP+ fascicles are enveloped by E10.5-R *Ascl1*$^{Cre\text{-}E}$+ cells and processes while adjacent fascicles are not (Figure 8I1-3; compare asterisks to arrowheads/arrow). Finally, fenestrated lamellar extensions of single *Ascl1*$^{Cre\text{-}E}$+ cells invest small fascicles of OMP+ axons (Figure 8J1-3). The distinctions between the relationship between *Ascl1*$^{Cre\text{-}E}$+ cells, NCAM+ and OMP+ axon fascicles suggests that a subpopulation of E10.5-R *Ascl1*$^{Cre\text{-}E}$+ olfactory ensheathing cells may interact with subsets of ORN axons.

DISCUSSION

Precursor cells in the early differentiating OE are distinguished by temporal as well as regional, molecular and proliferative characteristics (Figure 9A,B). We found a primarily dorsolateral population of Pax7+/Meis1+ precursors whose *Pax7*^{Cre}+ progeny initially appears biased to generate additional Pax7+ precursors and ORNs. We also identified a novel population of early generated dorsomedial Ascl1+ precursors that are not derived from Pax7+ precursors. A distinct cohort of these Ascl1+ precursors is labeled by conditional transcriptional lineage tracing via *Ascl1*$^{Cre\text{-}ERT}$ at E10.5. One day later, at E11.5, they remain as a spatially limited cohort of primarily proliferative precursors in the dorsomedial OE. Their non-proliferating progeny appear to be associated with the migratory mass adjacent to the coalescing ON in the fnm. At later fetal stages, these temporally, molecularly and regionally distinct Ascl1+ precursors generate subsets of medial and ventral ORNs as well as presumed sustentacular and ensheathing cells in the more anterior OE. Thus, from the outset of its differentiation, the OE comprises parallel precursor populations with distinct temporal and molecular signatures that bias their capacity to generate subsets of ORNs as well as other OE cell classes.

Cellular, molecular and genetic analysis of early OE precursors

Analysis of the early developing OE is complicated by its dynamic morphology, small size, and cellular diversity. The prevailing impression from many studies, including from our laboratory, has been that early OE precursors comprise unitary classes that progress through a singular lineage defined by expression of diagnostic transcription factors to generate ORNs and other OE cell types (reviewed by Beites et al., 2005; Moody and LaMantia, 2015; Schwob et al., 2017). We integrated constitutive and conditional transcriptional lineage tracing of two OE precursor populations to assess this impression: those expressing Pax7 (Murdoch et al, 2010) or Ascl1 (Cau et al., 2000; Cau et al., 1997; Gordon et al., 1995; Guillemot et al., 1993; Murray et al., 2003). We combined this analysis with quantitative assessment of additional transcription factors, proliferative activity, signaling, and cell identity (Figure 9A). OE progeny have been identified previously by constitutive *Pax7*^{Cre} (Murdoch et al., 2010), a *Six1* enhancer^{Cre} (Sato et al., 2015) or conditional *Isl1*$^{Cre\text{-}ERT}$ recombination (Taroc et al., 2020). Our combined *in vivo* and *in vitro* analyses of temporally, molecularly and regionally defined OE precursors in the mouse provide a complimentary view of OE precursor identity, lineage and fate to those defined by transcriptional lineage tracing in the mouse or electroporation of reporter and dominant-negative or gain-of-function constructs in chick embryos, where the nascent OE is accessible for such manipulation (Maier et al., 2010; Palaniappan et al., 2019). Our experiments cannot, however, account for broader molecular diversity among OE cells captured by transcriptomic analysis (Brunskill et al., 2014; Perera et al., 2020; Poopalasundaram et al., 2016).

Conditional fate mapping of OE progenitors at varying intervals has been used to evaluate *adult* OE neurogenesis or regeneration (Iwai et al., 2008; Leung et al., 2007; Packard et al., 2011). No published studies to our knowledge, however, have focused upon precursor identity over short intervals in the *developing* OE. The suggested central role of Ascl1 as a

regulator of transit amplifying terminally dividing ORN progenitors derived from upstream precursors (Cau et al., 2002; Guillemot et al., 1993; Murray et al., 2003; Tucker et al., 2010) led us to focus on *Ascl1*$^{Cre\text{-}ERT}$ conditional recombination for a dynamic view of OE precursor identities after two relatively short survival periods. Similar approaches have been used to assess temporally discrete Ascl1+ precursors and progeny in the spinal cord, cerebellum, and cerebral cortex (Allaway et al., 2020; Battiste et al., 2007; Kim et al., 2008; Sudarov et al., 2011; Vue et al., 2014). We also attempted conditional recombination using *Pax7*$^{Cre\text{-}ERT}$ in the E10.5 OE. Recombination was seen in lateral fnm at E11.5, as expected based upon Pax7 localization (LaMantia et al., 2000; Stoykova and Gruss, 1994). We did not, however, identify *Pax7*$^{Cre\text{-}E}$+ OE cells at E11.5 or E16.5 using two distinct *Pax7*$^{Cre\text{-}ERT}$ lines (Lepper et al., 2009; Lepper and Fan, 2010; Murphy et al., 2011). This may reflect incomplete Cre expression from the *Pax7* locus in distinct cell types or low recombination probability in slowly proliferating OE progenitors. Our findings from one temporally distinct, molecularly and positionally defined lineage cohort will need to be extended to better understand OE precursor diversity and its consequences.

Molecular versus temporal OE precursor diversity

Most analyses define OE precursor diversity primarily by expression of molecular determinants—particularly bHLH transcription factors like Ascl1, Ngn2, Hes1, and NeuroD (reviewed by Kam et al., 2014). Less attention has been paid to temporal diversity. The E10.5-R *Ascl1*$^{Cre\text{-}E}$+ precursor population we identify could not be recognized or followed based upon molecular marker expression. Time, in this instance, has substantial consequences for otherwise indistinguishable precursors and their progeny (Figure 9B). During the course of early OE differentiation, signals from neural crest-derived mesenchyme or adjacent cranial ectoderm (Bhasin et al., 2003; Forni et al., 2013; LaMantia et al., 2000; Szabo-Rogers et al., 2009; Whitesides et al., 1998), the OE itself (Gokoffski et al., 2011; Maier et al., 2011; Maier et al., 2010; Sabado et al., 2012) and amniotic fluid at the apical OE surface (Chau et al., 2015) are available to subsets of OE precursors. Thus, at any time during OE morphogenesis, any single OE precursor is likely influenced by a positionally distinct, concentration-dependent signaling matrix that establishes or constrains subsequent proliferation or differentiation. Nasal morphogenesis and growth may change this signaling matrix over time, continuously “updating” identities in temporal/spatial lineage cohorts.

Spatial restriction of the *Ascl1*$^{Cre\text{-}E}$+ OE transcriptional lineage cohort we identified here, as well as enhanced expression of pSMAD among these cells, suggests that subsets of OE progenitors may be specified within a signaling matrix that includes Bmps from both OE-intrinsic and extrinsic sources (Chau et al., 2015; LaMantia et al., 2000; Maier et al., 2010; Panaliappan et al., 2018). The localization of Bmps, especially Bmp4, in fnm and cranial ectoderm (LaMantia et al., 2000; Shou et al., 2000), Bmp4’s differential effects on OE neurogenesis (LaMantia et al., 2000; Maier et al., 2010; Panaliappan et al., 2018; Zhu et al., 2016) and enhanced frequency of pSMAD+ cells in E10.5-R *Ascl1*$^{Cre\text{-}E}$+ dorsomedial precursors are consistent with previous observations that Bmps or other Tgfβ signals influence OE neurogenesis and differentiation. Additional signals, including Retinoic Acid, Sonic hedgehog, Fgf8, Wnts and Notch may also influence temporally and spatially distinct OE precursor cohorts (Balmer and LaMantia, 2004; Herrick et al., 2018; Lassiter et

al., 2014; Maier et al., 2011; Rawson and LaMantia, 2007; Schwarting et al., 2007; Tucker et al., 2010; Whitesides et al., 1998). Recent work shows that subsets of Fgf20+ OE precursors, further regulated by Wnt signals, guide OE turbinate morphogenesis (Yang et al., 2018). Thus, serial signaling via multiple diffusible signals may integrate position and time to dynamically specify OE lineage cohorts by signaling state rather than singular expression of any particular molecular determinant.

Temporally distinct OE precursor cohorts and OE cellular diversity

Temporally distinct OE precursor cohorts may contribute to the regional or "zonal" organization of ORNs distinguished by monoallelic odorant receptor expression and segregated OB projections (Buck, 1996; Mori et al., 2000; Ressler et al., 1993; Vassar et al., 1993; Zapiec and Mombaerts, 2020). E10.5-R *Ascl1*$^{\text{Cre-E}}$+ precursor progeny identified at E16.5 includes a subset of ORNs limited to OE regions that correspond approximately to Zone 1 (reviewd by Mori et al., 2000) or the more recently defined Zolf24/Zolf16 (Zapiec and Mombaerts, 2020). The E10.5-R *Ascl1*$^{\text{Cre-E}}$+ lineage cohort may generate a "pioneer" population of Zone 1 ORNs to establish a template for additional zonal ORNs, or even non-neuronal cells, as they are added or regenerated. Whether ORNs generated by temporally distinct *Ascl1*$^{\text{Cre-E}}$+ precursors endure beyond fetal life, or a small number of precursors from this cohort continue to generate distinct OE cell types during OE maturation or ongoing regeneration remains to be determined. A more detailed understanding of temporal diversity of OE precursor lineages and cellular diversity is clearly necessary to better predict consequences of OE pathogenesis targeted to distinct cell classes (Cooper et al., 2020) and to optimize OE regeneration and functional recovery.

An early cohort of migratory mass cells are likely generated by the *Ascl1*$^{\text{Cre-E}}$+ OE lineage cohort (Figure 9). The absence of Ascl1 expression from the fnm, which is largely derived from neural crest (Karpinski et al., 2016; Osumi-Yamashita et al., 1994; Serbedzija et al., 1992) and the subset of E10.5-R *Ascl1*$^{\text{Cre-E}}$+ fnm cells at E11.5 suggest that early migratory mass cells are not generated solely by fnm neural crest (Barraud et al., 2010; Forni et al., 2011; Katoh et al., 2011). Instead, our current *in vivo* data are consistent with *in vitro* and *in vivo* observations that an initial population of migratory mass cells is generated primarily from olfactory placodal ectoderm (Karpinski et al., 2016; LaMantia et al., 2000; Miller et al., 2010; Rawson et al., 2010). E10.5-R *Ascl1*$^{\text{Cre-E}}$+ OE precursors generate substantial populations of E16.5 OE cells that express neither NCAM nor OMP. These cells include presumed sustentacular and ensheathing cells with distinct relationships with subsets of growing (NCAM+) as well as more mature (OMP+) ORN axons. Thus, sustentacular or ensheathing cell identity may be restricted in register with lineage-related ORN cohorts. Such a relationship, in concert with developmental and activity-dependent mechanisms, might facilitate subsequent high-fidelity regeneration of ORNs, their axons (Gogos et al., 2000), and adjacent ensheathing cells based upon lineage-related affinities.

Supplementary Material

Refer to Web version on PubMed Central for supplementary material.

ACKNOWLEDGEMENTS

This work was supported by NIDCD DC011534 and NICHD HD083157 to A-S. L. We thank Anastas Popratiloff and the staff of the GW Nanofabrication and Imaging Center for assistance with confocal microscopic imaging. We thank Mike Fox for thoughtful comments and Connor Siggins for proofreading the manuscript.

REFERENCES

Allaway KC, Munoz W, Tremblay R, Sherer M, Herron J, Rudy B, Machold R, Fishell G, 2020. Cellular birthdate predicts laminar and regional cholinergic projection topography in the forebrain. Elife 9.

Anchan RM, Drake DP, Haines CF, Gerwe EA, LaMantia AS, 1997. Disruption of local retinoid-mediated gene expression accompanies abnormal development in the mammalian olfactory pathway. J Comp Neurol 379, 171–184. [PubMed: 9050783]

Balmer CW, LaMantia AS, 2004. Loss of Gli3 and Shh function disrupts olfactory axon trajectories. J Comp Neurol 472, 292–307. [PubMed: 15065125]

Balmer CW, LaMantia AS, 2005. Noses and neurons: induction, morphogenesis, and neuronal differentiation in the peripheral olfactory pathway. Dev Dyn 234, 464–481. [PubMed: 16193510]

Barraud P, Seferiadis AA, Tyson LD, Zwart MF, Szabo-Rogers HL, Ruhrberg C, Liu KJ, Baker CV, 2010. Neural crest origin of olfactory ensheathing glia. Proc Natl Acad Sci U S A 107, 21040–21045. [PubMed: 21078992]

Bassett EA, Wallace VA, 2012. Cell fate determination in the vertebrate retina. Trends Neurosci 35, 565–573. [PubMed: 22704732]

Battiste J, Helms AW, Kim EJ, Savage TK, Lagace DC, Mandyam CD, Eisch AJ, Miyoshi G, Johnson JE, 2007. Ascl1 defines sequentially generated lineage-restricted neuronal and oligodendrocyte precursor cells in the spinal cord. Development 134, 285–293. [PubMed: 17166924]

Beites CL, Kawauchi S, Crocker CE, Calof AL, 2005. Identification and molecular regulation of neural stem cells in the olfactory epithelium. Exp Cell Res 306, 309–316. [PubMed: 15925585]

Bhasin N, Maynard TM, Gallagher PA, LaMantia AS, 2003. Mesenchymal/epithelial regulation of retinoic acid signaling in the olfactory placode. Dev Biol 261, 82–98. [PubMed: 12941622]

Brann DH, Tsukahara T, Weinreb C, Lipovsek M, Van den Berge K, Gong B, Chance R, Macaulay IC, Chou HJ, Fletcher RB, Das D, Street K, de Bezieux HR, Choi YG, Risso D, Dudoit S, Purdom E, Mill J, Hachem RA, Matsunami H, Logan DW, Goldstein BJ, Grubb MS, Ngai J, Datta SR, 2020. Non-neuronal expression of SARS-CoV-2 entry genes in the olfactory system suggests mechanisms underlying COVID-19-associated anosmia. Sci Adv 6.

Brunskill EW, Potter AS, Distasio A, Dexheimer P, Plassard A, Aronow BJ, Potter SS, 2014. A gene expression atlas of early craniofacial development. Dev Biol 391, 133–146. [PubMed: 24780627]

Buck LB, 1996. Information coding in the vertebrate olfactory system. Annu Rev Neurosci 19, 517–544. [PubMed: 8833453]

Byerly MS, Blackshaw S, 2009. Vertebrate retina and hypothalamus development. Wiley Interdiscip Rev Syst Biol Med 1, 380–389. [PubMed: 20836003]

Cau E, Casarosa S, Guillemot F, 2002. Mash1 and Ngn1 control distinct steps of determination and differentiation in the olfactory sensory neuron lineage. Development 129, 1871–1880. [PubMed: 11934853]

Cau E, Gradwohl G, Casarosa S, Kageyama R, Guillemot F, 2000. Hes genes regulate sequential stages of neurogenesis in the olfactory epithelium. Development 127, 2323–2332. [PubMed: 10804175]

Cau E, Gradwohl G, Fode C, Guillemot F, 1997. Mash1 activates a cascade of bHLH regulators in olfactory neuron progenitors. Development 124, 1611–1621. [PubMed: 9108377]

Chau KF, Springel MW, Broadbelt KG, Park HY, Topal S, Lun MP, Mullan H, Maynard T, Steen H, LaMantia AS, Lehtinen MK, 2015. Progressive Differentiation and Instructive Capacities of Amniotic Fluid and Cerebrospinal Fluid Proteomes following Neural Tube Closure. Dev Cell 35, 789–802. [PubMed: 26702835]

Chen B, Kim EH, Xu PX, 2009. Initiation of olfactory placode development and neurogenesis is blocked in mice lacking both Six1 and Six4. Dev Biol 326, 75–85. [PubMed: 19027001]

Child KM, Herrick DB, Schwob JE, Holbrook EH, Jang W, 2018. The Neuroregenerative Capacity of Olfactory Stem Cells Is Not Limitless: Implications for Aging. J Neurosci 38, 6806–6824. [PubMed: 29934351]

Coleman JH, Lin B, Louie JD, Peterson J, Lane RP, Schwob JE, 2019. Spatial Determination of Neuronal Diversification in the Olfactory Epithelium. J Neurosci 39, 814–832. [PubMed: 30530861]

Cooper KW, Brann DH, Farruggia MC, Bhutani S, Pellegrino R, Tsukahara T, Weinreb C, Joseph PV, Larson ED, Parma V, Albers MW, Barlow LA, Datta SR, Di Pizio A, 2020. COVID-19 and the Chemical Senses: Supporting Players Take Center Stage. Neuron 107, 219–233. [PubMed: 32640192]

Dincer Z, Piao J, Niu L, Ganat Y, Kriks S, Zimmer B, Shi SH, Tabar V, Studer L, 2013. Specification of functional cranial placode derivatives from human pluripotent stem cells. Cell Rep 5, 1387–1402. [PubMed: 24290755]

Donner AL, Episkopou V, Maas RL, 2007. Sox2 and Pou2f1 interact to control lens and olfactory placode development. Dev Biol 303, 784–799. [PubMed: 17140559]

Ellis P, Fagan BM, Magness ST, Hutton S, Taranova O, Hayashi S, McMahon A, Rao M, Pevny L, 2004. SOX2, a persistent marker for multipotential neural stem cells derived from embryonic stem cells, the embryo or the adult. Dev Neurosci 26, 148–165. [PubMed: 15711057]

Forni PE, Bharti K, Flannery EM, Shimogori T, Wray S, 2013. The indirect role of fibroblast growth factor-8 in defining neurogenic niches of the olfactory/GnRH systems. J Neurosci 33, 19620–19634. [PubMed: 24336726]

Forni PE, Taylor-Burds C, Melvin VS, Williams T, Wray S, 2011. Neural crest and ectodermal cells intermix in the nasal placode to give rise to GnRH-1 neurons, sensory neurons, and olfactory ensheathing cells. J Neurosci 31, 6915–6927. [PubMed: 21543621]

Franssen EH, de Bree FM, Verhaagen J, 2007. Olfactory ensheathing glia: their contribution to primary olfactory nervous system regeneration and their regenerative potential following transplantation into the injured spinal cord. Brain Res Rev 56, 236–258. [PubMed: 17884174]

Fritzsch B, Beisel KW, Jones K, Farinas I, Maklad A, Lee J, Reichardt LF, 2002. Development and evolution of inner ear sensory epithelia and their innervation. J Neurobiol 53, 143–156. [PubMed: 12382272]

Gogos JA, Osborne J, Nemes A, Mendelsohn M, Axel R, 2000. Genetic ablation and restoration of the olfactory topographic map. Cell 103, 609–620. [PubMed: 11106731]

Gokoffski KK, Wu HH, Beites CL, Kim J, Kim EJ, Matzuk MM, Johnson JE, Lander AD, Calof AL, 2011. Activin and GDF11 collaborate in feedback control of neuroepithelial stem cell proliferation and fate. Development 138, 4131–4142. [PubMed: 21852401]

Gordon MK, Mumm JS, Davis RA, Holcomb JD, Calof AL, 1995. Dynamics of MASH1 expression in vitro and in vivo suggest a non-stem cell site of MASH1 action in the olfactory receptor neuron lineage. Mol Cell Neurosci 6, 363–379. [PubMed: 8846005]

Graziadei GA, Stanley RS, Graziadei PP, 1980. The olfactory marker protein in the olfactory system of the mouse during development. Neuroscience 5, 1239–1252. [PubMed: 7402467]

Guillemot F, Joyner AL, 1993. Dynamic expression of the murine Achaete-Scute homologue Mash-1 in the developing nervous system. Mech Dev 42, 171–185. [PubMed: 8217843]

Guillemot F, Lo LC, Johnson JE, Auerbach A, Anderson DJ, Joyner AL, 1993. Mammalian achaete-scute homolog 1 is required for the early development of olfactory and autonomic neurons. Cell 75, 463–476. [PubMed: 8221886]

Guo Z, Packard A, Krolewski RC, Harris MT, Manglapus GL, Schwob JE, 2010. Expression of pax6 and sox2 in adult olfactory epithelium. J Comp Neurol 518, 4395–4418. [PubMed: 20852734]

Hegarty SV, O'Keeffe GW, Sullivan AM, 2013. BMP-Smad 1/5/8 signalling in the development of the nervous system. Prog Neurobiol 109, 28–41. [PubMed: 23891815]

Herrick DB, Guo Z, Jang W, Schnittke N, Schwob JE, 2018. Canonical Notch Signaling Directs the Fate of Differentiating Neurocompetent Progenitors in the Mammalian Olfactory Epithelium. J Neurosci 38, 5022–5037. [PubMed: 29739871]

Horie R, Hazbun A, Chen K, Cao C, Levine M, Horie T, 2018. Shared evolutionary origin of vertebrate neural crest and cranial placodes. Nature 560, 228–232. [PubMed: 30069052]

Ikeda K, Kageyama R, Suzuki Y, Kawakami K, 2010. Six1 is indispensable for production of functional progenitor cells during olfactory epithelial development. Int J Dev Biol 54, 1453–1464. [PubMed: 21302255]

Ikeda K, Ookawara S, Sato S, Ando Z, Kageyama R, Kawakami K, 2007. Six1 is essential for early neurogenesis in the development of olfactory epithelium. Dev Biol 311, 53–68. [PubMed: 17880938]

Iwai N, Zhou Z, Roop DR, Behringer RR, 2008. Horizontal basal cells are multipotent progenitors in normal and injured adult olfactory epithelium. Stem Cells 26, 1298–1306. [PubMed: 18308944]

Kam JW, Raja R, Cloutier JF, 2014. Cellular and molecular mechanisms regulating embryonic neurogenesis in the rodent olfactory epithelium. Int J Dev Neurosci 37, 76–86. [PubMed: 25003986]

Karpinski BA, Bryan CA, Paronett EM, Baker JL, Fernandez A, Horvath A, Maynard TM, Moody SA, LaMantia AS, 2016. A cellular and molecular mosaic establishes growth and differentiation states for cranial sensory neurons. Dev Biol 415, 228–241. [PubMed: 26988119]

Katoh H, Shibata S, Fukuda K, Sato M, Satoh E, Nagoshi N, Minematsu T, Matsuzaki Y, Akazawa C, Toyama Y, Nakamura M, Okano H, 2011. The dual origin of the peripheral olfactory system: placode and neural crest. Mol Brain 4, 34. [PubMed: 21943152]

Keller C, Hansen MS, Coffin CM, Capecchi MR, 2004. Pax3:Fkhr interferes with embryonic Pax3 and Pax7 function: implications for alveolar rhabdomyosarcoma cell of origin. Genes Dev 18, 2608–2613. [PubMed: 15520281]

Khan M, Yoo SJ, Clijsters M, Backaert W, Vanstapel A, Speleman K, Lietaer C, Choi S, Hether TD, Marcelis L, Nam A, Pan L, Reeves JW, Van Bulck P, Zhou H, Bourgeois M, Debaveye Y, De Munter P, Gunst J, Jorissen M, Lagrou K, Lorent N, Neyrinck A, Peetermans M, Thal DR, Vandenbriele C, Wauters J, Mombaerts P, Van Gerven L, 2021. Visualizing in deceased COVID-19 patients how SARS-CoV-2 attacks the respiratory and olfactory mucosae but spares the olfactory bulb. Cell 184, 5932–5949 e5915. [PubMed: 34798069]

Kim EJ, Battiste J, Nakagawa Y, Johnson JE, 2008. Ascl1 (Mash1) lineage cells contribute to discrete cell populations in CNS architecture. Mol Cell Neurosci 38, 595–606. [PubMed: 18585058]

LaMantia AS, 2020. Why Does the Face Predict the Brain? Neural Crest Induction, Craniofacial Morphogenesis, and Neural Circuit Development. Front Physiol 11, 610970. [PubMed: 33362582]

LaMantia AS, Bhasin N, Rhodes K, Heemskerk J, 2000. Mesenchymal/epithelial induction mediates olfactory pathway formation. Neuron 28, 411–425. [PubMed: 11144352]

LaMantia AS, Colbert MC, Linney E, 1993. Retinoic acid induction and regional differentiation prefigure olfactory pathway formation in the mammalian forebrain. Neuron 10, 1035–1048. [PubMed: 8318228]

Lassiter RN, Stark MR, Zhao T, Zhou CJ, 2014. Signaling mechanisms controlling cranial placode neurogenesis and delamination. Dev Biol 389, 39–49. [PubMed: 24315854]

Lehtinen MK, Zappaterra MW, Chen X, Yang YJ, Hill AD, Lun M, Maynard T, Gonzalez D, Kim S, Ye P, D'Ercole AJ, Wong ET, LaMantia AS, Walsh CA, 2011. The cerebrospinal fluid provides a proliferative niche for neural progenitor cells. Neuron 69, 893–905. [PubMed: 21382550]

Lepper C, Conway SJ, Fan CM, 2009. Adult satellite cells and embryonic muscle progenitors have distinct genetic requirements. Nature 460, 627–631. [PubMed: 19554048]

Lepper C, Fan CM, 2010. Inducible lineage tracing of Pax7-descendant cells reveals embryonic origin of adult satellite cells. Genesis 48, 424–436. [PubMed: 20641127]

Leung CT, Coulombe PA, Reed RR, 2007. Contribution of olfactory neural stem cells to tissue maintenance and regeneration. Nat Neurosci 10, 720–726. [PubMed: 17468753]

Liang F, 2018. Olfactory receptor neuronal dendrites become mostly intra-sustentacularly enwrapped upon maturity. J Anat 232, 674–685. [PubMed: 29313978]

Liberia T, Martin-Lopez E, Meller SJ, Greer CA, 2019. Sequential Maturation of Olfactory Sensory Neurons in the Mature Olfactory Epithelium. eNeuro 6.

Madisen L, Zwingman TA, Sunkin SM, Oh SW, Zariwala HA, Gu H, Ng LL, Palmiter RD, Hawrylycz MJ, Jones AR, Lein ES, Zeng H, 2010. A robust and high-throughput Cre reporting

and characterization system for the whole mouse brain. Nat Neurosci 13, 133–140. [PubMed: 20023653]

Maier E, Nord H, von Hofsten J, Gunhaga L, 2011. A balance of BMP and notch activity regulates neurogenesis and olfactory nerve formation. PLoS One 6, e17379. [PubMed: 21383851]

Maier E, von Hofsten J, Nord H, Fernandes M, Paek H, Hebert JM, Gunhaga L, 2010. Opposing Fgf and Bmp activities regulate the specification of olfactory sensory and respiratory epithelial cell fates. Development 137, 1601–1611. [PubMed: 20392740]

Miller AM, Treloar HB, Greer CA, 2010. Composition of the migratory mass during development of the olfactory nerve. J Comp Neurol 518, 4825–4841. [PubMed: 21031554]

Miragall F, Dermietzel R, 1992. Immunocytochemical localization of cell adhesion molecules in the developing and mature olfactory system. Microsc Res Tech 23, 157–172. [PubMed: 1384811]

Miragall F, Kadmon G, Schachner M, 1989. Expression of L1 and N-CAM cell adhesion molecules during development of the mouse olfactory system. Dev Biol 135, 272–286. [PubMed: 2776969]

Monahan K, Lomvardas S, 2015. Monoallelic expression of olfactory receptors. Annu Rev Cell Dev Biol 31, 721–740. [PubMed: 26359778]

Moody SA, LaMantia AS, 2015. Transcriptional regulation of cranial sensory placode development. Curr Top Dev Biol 111, 301–350. [PubMed: 25662264]

Mori K, von Campenhause H, Yoshihara Y, 2000. Zonal organization of the mammalian main and accessory olfactory systems. Philos Trans R Soc Lond B Biol Sci 355, 1801–1812. [PubMed: 11205342]

Morse WR, Whitesides JG 3rd, LaMantia AS, Maness PF, 1998. p59fyn and pp60c-src modulate axonal guidance in the developing mouse olfactory pathway. J Neurobiol 36, 53–63. [PubMed: 9658338]

Murdoch B, DelConte C, Garcia-Castro MI, 2010. Embryonic Pax7-expressing progenitors contribute multiple cell types to the postnatal olfactory epithelium. J Neurosci 30, 9523–9532. [PubMed: 20631180]

Murphy MM, Lawson JA, Mathew SJ, Hutcheson DA, Kardon G, 2011. Satellite cells, connective tissue fibroblasts and their interactions are crucial for muscle regeneration. Development 138, 3625–3637. [PubMed: 21828091]

Murray RC, Navi D, Fesenko J, Lander AD, Calof AL, 2003. Widespread defects in the primary olfactory pathway caused by loss of Mash1 function. J Neurosci 23, 1769–1780. [PubMed: 12629181]

Osumi-Yamashita N, Ninomiya Y, Doi H, Eto K, 1994. The contribution of both forebrain and midbrain crest cells to the mesenchyme in the frontonasal mass of mouse embryos. Dev Biol 164, 409–419. [PubMed: 8045344]

Packard A, Giel-Moloney M, Leiter A, Schwob JE, 2011. Progenitor cell capacity of NeuroD1-expressing globose basal cells in the mouse olfactory epithelium. J Comp Neurol 519, 3580–3596. [PubMed: 21800309]

Packard AI, Lin B, Schwob JE, 2016. Sox2 and Pax6 Play Counteracting Roles in Regulating Neurogenesis within the Murine Olfactory Epithelium. PLoS One 11, e0155167. [PubMed: 27171428]

Palaniappan TK, Slekiene L, Gunhaga L, Patthey C, 2019. Extensive apoptosis during the formation of the terminal nerve ganglion by olfactory placode-derived cells with distinct molecular markers. Differentiation 110, 8–16. [PubMed: 31539705]

Panaliappan TK, Wittmann W, Jidigam VK, Mercurio S, Bertolini JA, Sghari S, Bose R, Patthey C, Nicolis SK, Gunhaga L, 2018. Sox2 is required for olfactory pit formation and olfactory neurogenesis through BMP restriction and Hes5 upregulation. Development 145.

Parras CM, Schuurmans C, Scardigli R, Kim J, Anderson DJ, Guillemot F, 2002. Divergent functions of the proneural genes Mash1 and Ngn2 in the specification of neuronal subtype identity. Genes Dev 16, 324–338. [PubMed: 11825874]

Perera SN, Williams RM, Lyne R, Stubbs O, Buehler DP, Sauka-Spengler T, Noda M, Micklem G, Southard-Smith EM, Baker CVH, 2020. Insights into olfactory ensheathing cell development from a laser-microdissection and transcriptome-profiling approach. Glia 68, 2550–2584. [PubMed: 32857879]

Poopalasundaram S, Chambers D, Graham A, Bouloux PM, 2016. Serotonin Receptor 1A (HTR1A), a Novel Regulator of GnRH Neuronal Migration in Chick Embryo. Endocrinology 157, 4632–4640. [PubMed: 27732089]

Rawson NE, LaMantia AS, 2007. A speculative essay on retinoic acid regulation of neural stem cells in the developing and aging olfactory system. Exp Gerontol 42, 46–53. [PubMed: 16860961]

Rawson NE, Lischka FW, Yee KK, Peters AZ, Tucker ES, Meechan DW, Zirlinger M, Maynard TM, Burd GB, Dulac C, Pevny L, LaMantia AS, 2010. Specific mesenchymal/epithelial induction of olfactory receptor, vomeronasal, and gonadotropin-releasing hormone (GnRH) neurons. Dev Dyn 239, 1723–1738. [PubMed: 20503368]

Ressler KJ, Sullivan SL, Buck LB, 1993. A zonal organization of odorant receptor gene expression in the olfactory epithelium. Cell 73, 597–609. [PubMed: 7683976]

Rigby MJ, Gomez TM, Puglielli L, 2020. Glial Cell-Axonal Growth Cone Interactions in Neurodevelopment and Regeneration. Front Neurosci 14, 203. [PubMed: 32210757]

Rodriguez I, 2013. Singular expression of olfactory receptor genes. Cell 155, 274–277. [PubMed: 24120129]

Roskams AJ, Cai X, Ronnett GV, 1998. Expression of neuron-specific beta-III tubulin during olfactory neurogenesis in the embryonic and adult rat. Neuroscience 83, 191–200. [PubMed: 9466409]

Sabado V, Barraud P, Baker CV, Streit A, 2012. Specification of GnRH-1 neurons by antagonistic FGF and retinoic acid signaling. Dev Biol 362, 254–262. [PubMed: 22200593]

Salazar I, Sanchez-Quinteiro P, Barrios AW, Lopez Amado M, Vega JA, 2019. Anatomy of the olfactory mucosa. Handb Clin Neurol 164, 47–65. [PubMed: 31604563]

Sato S, Yajima H, Furuta Y, Ikeda K, Kawakami K, 2015. Activation of Six1 Expression in Vertebrate Sensory Neurons. PLoS One 10, e0136666. [PubMed: 26313368]

Schlosser G, Patthey C, Shimeld SM, 2014. The evolutionary history of vertebrate cranial placodes II. Evolution of ectodermal patterning. Dev Biol 389, 98–119. [PubMed: 24491817]

Schwarting GA, Gridley T, Henion TR, 2007. Notch1 expression and ligand interactions in progenitor cells of the mouse olfactory epithelium. J Mol Histol 38, 543–553. [PubMed: 17605079]

Schwob JE, 2002. Neural regeneration and the peripheral olfactory system. Anat Rec 269, 33–49. [PubMed: 11891623]

Schwob JE, Jang W, Holbrook EH, Lin B, Herrick DB, Peterson JN, Hewitt Coleman J, 2017. Stem and progenitor cells of the mammalian olfactory epithelium: Taking poietic license. J Comp Neurol 525, 1034–1054. [PubMed: 27560601]

Serbedzija GN, Bronner-Fraser M, Fraser SE, 1992. Vital dye analysis of cranial neural crest cell migration in the mouse embryo. Development 116, 297–307. [PubMed: 1283734]

Shen Q, Zhong W, Jan YN, Temple S, 2002. Asymmetric Numb distribution is critical for asymmetric cell division of mouse cerebral cortical stem cells and neuroblasts. Development 129, 4843–4853. [PubMed: 12361975]

Shiau F, Ruzycki PA, Clark BS, 2021. A single-cell guide to retinal development: Cell fate decisions of multipotent retinal progenitors in scRNA-seq. Dev Biol 478, 41–58. [PubMed: 34146533]

Shou J, Murray RC, Rim PC, Calof AL, 2000. Opposing effects of bone morphogenetic proteins on neuron production and survival in the olfactory receptor neuron lineage. Development 127, 5403–5413. [PubMed: 11076761]

Shou J, Rim PC, Calof AL, 1999. BMPs inhibit neurogenesis by a mechanism involving degradation of a transcription factor. Nat Neurosci 2, 339–345. [PubMed: 10204540]

Sokpor G, Abbas E, Rosenbusch J, Staiger JF, Tuoc T, 2018. Transcriptional and Epigenetic Control of Mammalian Olfactory Epithelium Development. Mol Neurobiol 55, 8306–8327. [PubMed: 29532253]

Stoykova A, Gruss P, 1994. Roles of Pax-genes in developing and adult brain as suggested by expression patterns. J Neurosci 14, 1395–1412. [PubMed: 8126546]

Sudarov A, Turnbull RK, Kim EJ, Lebel-Potter M, Guillemot F, Joyner AL, 2011. Ascl1 genetics reveals insights into cerebellum local circuit assembly. J Neurosci 31, 11055–11069. [PubMed: 21795554]

Sullivan SL, Bohm S, Ressler KJ, Horowitz LF, Buck LB, 1995. Target-independent pattern specification in the olfactory epithelium. Neuron 15, 779–789. [PubMed: 7576628]

Szabo-Rogers HL, Geetha-Loganathan P, Whiting CJ, Nimmagadda S, Fu K, Richman JM, 2009. Novel skeletogenic patterning roles for the olfactory pit. Development 136, 219–229. [PubMed: 19056832]

Taroc EZM, Katreddi RR, Forni PE, 2020. Identifying Isl1 Genetic Lineage in the Developing Olfactory System and in GnRH-1 Neurons. Front Physiol 11, 601923. [PubMed: 33192618]

Toresson H, Parmar M, Campbell K, 2000a. Expression of Meis and Pbx genes and their protein products in the developing telencephalon: implications for regional differentiation. Mech Dev 94, 183–187. [PubMed: 10842069]

Toresson H, Potter SS, Campbell K, 2000b. Genetic control of dorsal-ventral identity in the telencephalon: opposing roles for Pax6 and Gsh2. Development 127, 4361–4371. [PubMed: 11003836]

Tucker ES, Lehtinen MK, Maynard T, Zirlinger M, Dulac C, Rawson N, Pevny L, Lamantia AS, 2010. Proliferative and transcriptional identity of distinct classes of neural precursors in the mammalian olfactory epithelium. Development 137, 2471–2481. [PubMed: 20573694]

Vassar R, Ngai J, Axel R, 1993. Spatial segregation of odorant receptor expression in the mammalian olfactory epithelium. Cell 74, 309–318. [PubMed: 8343958]

von Bohlen und Halbach O, 2011. Immunohistological markers for proliferative events, gliogenesis, and neurogenesis within the adult hippocampus. Cell Tissue Res 345, 1–19. [PubMed: 21647561]

Vue TY, Kim EJ, Parras CM, Guillemot F, Johnson JE, 2014. Ascl1 controls the number and distribution of astrocytes and oligodendrocytes in the gray matter and white matter of the spinal cord. Development 141, 3721–3731. [PubMed: 25249462]

Ware M, Hamdi-Roze H, Le Friec J, David V, Dupe V, 2016. Regulation of downstream neuronal genes by proneural transcription factors during initial neurogenesis in the vertebrate brain. Neural Dev 11, 22. [PubMed: 27923395]

Whitesides J, Hall M, Anchan R, LaMantia AS, 1998. Retinoid signaling distinguishes a subpopulation of olfactory receptor neurons in the developing and adult mouse. J Comp Neurol 394, 445–461. [PubMed: 9590554]

Whitesides JG 3rd, LaMantia AS, 1996. Differential adhesion and the initial assembly of the mammalian olfactory nerve. J Comp Neurol 373, 240–254. [PubMed: 8889925]

Wu HH, Ivkovic S, Murray RC, Jaramillo S, Lyons KM, Johnson JE, Calof AL, 2003. Autoregulation of neurogenesis by GDF11. Neuron 37, 197–207. [PubMed: 12546816]

Yamashita H, Kawata K, Takahashi M, 1998. Upregulation of neural growth-associated protein and neural cell adhesion molecule in mouse olfactory epithelium and axons after unilateral removal of the olfactory bulb. Eur Arch Otorhinolaryngol 255, 441–445. [PubMed: 9833210]

Yang LM, Huh SH, Ornitz DM, 2018. FGF20-Expressing, Wnt-Responsive Olfactory Epithelial Progenitors Regulate Underlying Turbinate Growth to Optimize Surface Area. Dev Cell 46, 564–580 e565. [PubMed: 30100263]

Zapiec B, Mombaerts P, 2020. The Zonal Organization of Odorant Receptor Gene Choice in the Main Olfactory Epithelium of the Mouse. Cell Rep 30, 4220–4234 e4225. [PubMed: 32209480]

Zhu XJ, Liu Y, Yuan X, Wang M, Zhao W, Yang X, Zhang X, Hsu W, Qiu M, Zhang Z, Zhang Z, 2016. Ectodermal Wnt controls nasal pit morphogenesis through modulation of the BMP/FGF/JNK signaling axis. Dev Dyn 245, 414–426. [PubMed: 26661618]

Highlights

- At least two multipotent precursor classes in the nascent olfactory epithelium
- Timing, location, and divergent transcription factor expression defines precursors
- Ascl1 defines a temporally distinct medial olfactory epithelial precursor cohort
- Early Ascl1 medial precursors are biased to generate cells in the migratory mass
- Early Ascl1 precursors generate all cell types in the maturing olfactory epithelium

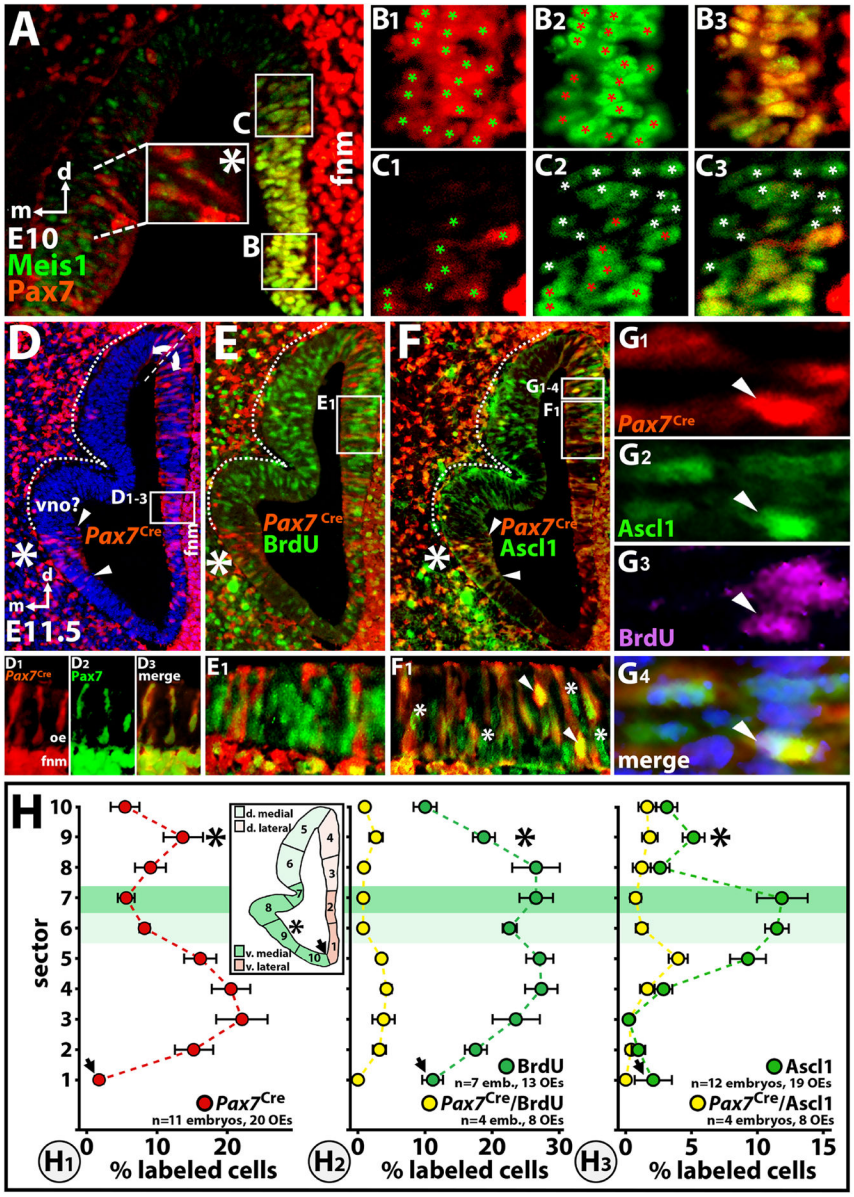

Figure 1:

Distribution and identities of early Pax7+ olfactory epithelial (OE) progenitors. **A**) Pax7+ cells (immunolabeled; red), coincide with Meis1+ cells (immunolabeled; green) in the E10.0 lateral OE (coronal section; d=dorsal, m=medial). A small population of Pax7+/Meis1− cells is also seen in the ventromedial OE (dotted lines, box, large asterisk). Pax7 is also seen in mesenchymal cells of the lateral frontonasal mesenchym (fnm). **B_{1-3}**) Registration of Pax7+ (red label, green asterisks; *panel* **1**) and Meis1+ (green label, red asterisks; *panel* **2**) cells in the ventrolateral OE (merged; *panel* **3**). **C_{1-3}**) A subset of dorsolateral Pax7+ cells (*panel* **1**) are co-labeled for Meis1+ (*panel* **2**). Single-labeled Meis1+ cells are indicated by white asterisks (merged; *panel* **3**). **D**) Cells labeled by a *Pax7*^{Cre}-recombined floxed tdTomato reporter (*Pax7*^{Cre}+) in the OE as well as fnm at E11.5 (coronal section). *Pax7*^{Cre}+ cells are most frequent in the lateral OE and frontonasal mesenchyme (fnm). The dashed

line across the dorsomedial OE and the arrows on either side of it indicate the variability likely between boundaries seen in individual sections the morphometric assessment of the distribution of *Pax7*^{Cre}+ cells (see panel 1H). There is also a small domain of *Pax7*^{Cre}+ cells in the ventromedial OE, mostly ventral to the region where the vomeronasal organ presumably will form (vno?; arrowheads, large asterisk). The dotted line (also shown in panels **E & F**) indicates the dorsomedial OE region where *Pax7*^{Cre}+ cells are rarely seen at E11.5. **D$_{1-3}$**) Registration of *Pax7*^{Cre}+ (red) and Pax7+ (green) cells in E11.5 lateral OE and fnm. **E**) Relationship of *Pax7*^{Cre}+ cells to proliferating OE precursors labeled acutely with BrdU, which are most frequent in the dorsal OE. **E1**) Lateral OE *Pax7*^{Cre}+ cells are distinct from BrdU+ cells. **F**) Dorsomedial Ascl1+ cells are mostly segregated from lateral *Pax7*^{Cre}+ OE cells (dotted line); however, occasional *Pax7*^{Cre}+/Ascl1+ cells are seen in the dorsolateral OE (boxes **F$_1$**, **G$_{1-4}$**), coincident with the region where BrdU+ cells are more frequent in the dorsolateral OE. *Pax7*^{Cre}+ and Ascl1+, but not BrdU+, cells also appear more frequently (arrowheads, large white asterisk) in the ventromedial region adjacent to the presumptive vno. **F$_1$**) In the dorsolateral OE, a subset of *Pax7*^{Cre}+ cells are also Ascl1+ (arrowheads); however, other Ascl1+ cells are *Pax7*^{Cre}- (asterisks). **G$_{1-4}$**) In the dorsolateral OE, occasional *Pax7*^{Cre}+ cells (arrowhead, **G$_1$**) are also Ascl1+ (arrowhead, **G$_2$**) and BrdU+ (arrowhead, **G$_3$**; merged image, arrowhead **G$_4$**). **H**) Relative frequency of *Pax7*^{Cre}+ (**H$_1$**), BrdU+ (**H$_2$**) and Ascl1+ cells (**H$_3$**), all as a proportion of total DAPI+ cells, measured in 10 linearly equivalent sectors (*inset*; see Methods & Results for additional explanation) with axial positions indicated by the color code and key. The arrow indicates the OE ventral nadir, where sector 1 begins (lateral) and sector 10 ends (medial). Numbers of embryos and OEs counted for each marker are shown. Error bars reflect standard error of the mean for each point. Light green shading across the graphs indicates dorsomedial sector 6 and darker green indicates sector 7 where BrdU+ and Ascl1+ cells are more frequent.

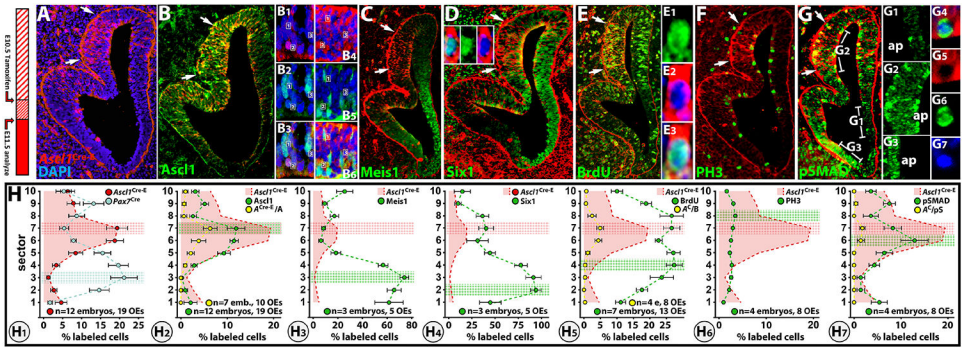

Figure 2:

A distinct zone of highly proliferative Ascl1+ descended precursors in the E11.5 OE. ***Far left***: the schedule of tamoxifen injection and embryo collection used to generate the data. **A**) After initiating recombination with a single E10.5 tamoxifen injection, there is a population of *Ascl1*$^{\text{Cre-E}}$+ cells (arrows) concentrated in the dorsomedial OE. **B**) Ascl1+ (protein) cells are mostly limited to the dorsomedial OE region where *Ascl1*$^{\text{Cre-E}}$+ cells are also concentrated. **B$_{1\text{-}3}$**) Dorsolateral Ascl1+ cells (boxes 1,3) are distinct from *Ascl1*$^{\text{Cre-E}}$+ cells (box 2). **B$_{4\text{-}6}$)** There are dorsomedial OE cells that are both Ascl1+/*Ascl1*$^{\text{Cre-E}}$+ (boxes 1,2) and Ascl1+/ *Ascl1*$^{\text{Cre-E}}$ – (box 3). **C**) *Ascl1*$^{\text{Cre-E}}$+ cells are segregated from Meis1+ lateral OE progenitors. **D**) Six1+ cells are substantially more frequent in the lateral OE, including in the region where *Pax7*$^{\text{Cre}}$+ cells are found. Some *Ascl1*$^{\text{Cre-E}}$+ cells are also Six1+ (*inset*). **E**) Dorsomedial *Ascl1*$^{\text{Cre-E}}$+ cells coincide with a dorsomedial region where actively proliferating BrdU+ cells are more frequent (arrows). **E$_{1\text{-}3}$**) *Ascl1*$^{\text{Cre-E}}$+ cells are also BrdU+. **F**) PH3+ (Phospho-Histone 3), presumably actively mitotic, cells are distributed fairly uniformly and at low frequency across the OE. **G**) Phosphorylated SMAD 1/5/8 (pSMAD)-labeled nuclei are found primarily in apical *Ascl1*$^{\text{Cre-E}}$+ dorsomedial OE cells. **G$_{1\text{-}3}$**) pSMAD+ cells are infrequent in the ventrolateral OE (**G$_1$**), and more frequent in the dorsomedial and extreme ventromedial OE (*G$_2$*, **G$_3$**). pSMAD+ cells are more frequent in the most apical (ap) as well as most basal regions of the OE. **G$_{4\text{-}6}$**) An apical *Ascl1*$^{\text{Cre-E}}$+ dorsomedial OE cell with a pSMAD+ nucleus. **H**) Quantitative analysis of multiple OE cell markers, relative to *Ascl1*$^{\text{Cre-E}}$ + cells using the sector analysis method (see Figure 1H). **H$_1$)** Relation of *Ascl1*$^{\text{Cre-E}}$ marked cells (red) relative to *Pax7*$^{\text{Cre}}$ cells (blue; data replotted from Figure 1H). In subsequent graphs, a “ghost” image of the Ascl1Cre-E+ cell distribution, scaled to the cell frequency of the additional cell population, is shown by the red hatched curve. **H$_{2\text{-}7}$)** Quantification of Meis1+, Six1+, Ascl1+, BrdU+, PH3+, and pSMAD+ cells, relative to *Ascl1*$^{\text{Cre-E}}$+ cells (red “ghost” curve). Hatched red and green bars indicate maximal frequency for the relevant cell classes. Yellow points (**H$_{4,\,5,7}$**) indicate percentages of cells double labeled for *Ascl1*$^{\text{Cre-E}}$+/ Ascl1+(protein), or BrdU+, and pSMAD+ cells.

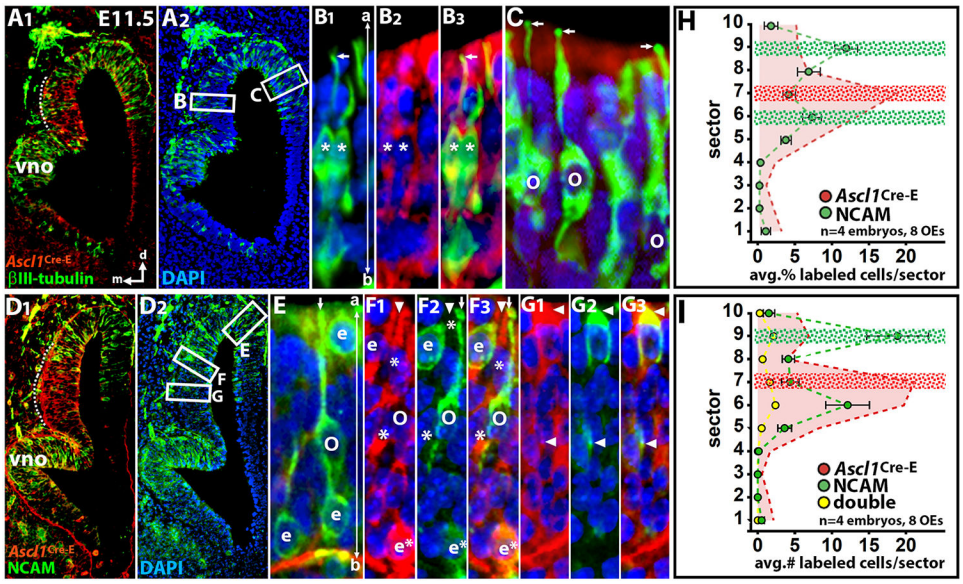

Figure 3:

The relationship between the distribution of early differentiating olfactory receptor neurons (ORNs) and *Ascl1*$^{Cre\text{-}E}$+ precursors. **A$_{1,2}$**) Early generated ORNs, labeled for the early neuronal marker βIII-tubulin (green, **A$_1$**, **A$_2$**), are distributed throughout the dorsolateral and dorsomedial OE. The frequency of βIII-tubulin+ presumptive ORNs appears to be attenuated in the region where *Ascl1*$^{Cre\text{-}E}$+ cells '(red, **A$_1$**) are found (dotted line). Boxes indicated regions enlarged in panels **B** and **C**. **B$_{1\text{-}3}$**) Subsets of βIII-tubulin+ ORNs with apically (ap) oriented dendrites are *Ascl1*$^{Cre\text{-}E}$+ (asterisks). **C**) βIII-tubulin+ ORNs (o) in more lateral regions are not *Ascl1*$^{Cre\text{-}E}$+. **D$_{1,2}$)** Relationship between the distribution of NCAM+ ORNs and *Ascl1*$^{Cre\text{-}E}$+ cells in the E11.5 OE. NCAM+ cells are mostly excluded from the region where *Ascl1*$^{Cre\text{-}E}$+ cells (red, **D$_1$**) are most frequent (dotted line). The regions boxed in **D$_2$** are enlarged in panels **E**, **F** and **G**. **E)** NCAM+/*Ascl*$^{Cre\text{-}E}$– cells in the dorsolateral OE have essential characteristics of ORNs (o), including apically oriented apparent dendrites and apparent dendritic knobs (arrow). They are often adjacent to NCAM+/*Ascl1*$^{Cre\text{-}E}$– apical (a) and basal (b) epithelial cells. (e). **F$_{1\text{-}3}$)** At the dorsal margin of the region where *Ascl1*$^{Cre\text{-}E}$+ cells are most frequent, NCAM+/*Ascl1*$^{Cre\text{-}E}$– cells are seen with cytological characteristics of ORNs (o) including a dendritic knob at the apical OE surface (arrow). There are also NCAM+ (e) and *Ascl1*$^{Cre\text{-}E}$+ (*) epithelial cells, some with apical processes (arrowhead). **G$_{1\text{-}3}$**) NCAM+/*Ascl1*$^{Cre\text{-}E}$+ as well as *Ascl1*$^{Cre\text{-}E}$+/NCAM- cells are seen in the apical and mid-OE (arrowheads) in the the region where *Ascl1*$^{Cre\text{-}}$E+ cells are concentrated. **H**) Sector plot of NCAM+ cell frequency (% DAPI+ cells/sector, green circles), with the distribution of *Ascl1*$^{Cre\text{-}E}$+ cells (red curve) for comparison. The sectors with peak frequency of NCAM+ and *Ascl1*$^{Cre\text{-}E}$+ cells are indicated with hatched horizontal green and red bars, respectively. **I**) Sector plot of absolute numbers of NCAM+ (green circles), *Ascl1*$^{Cre\text{-}E}$+ (red curve) and NCAM+/ *Ascl1*$^{Cre\text{-}E}$+ double-labeled cells (yellow circles).

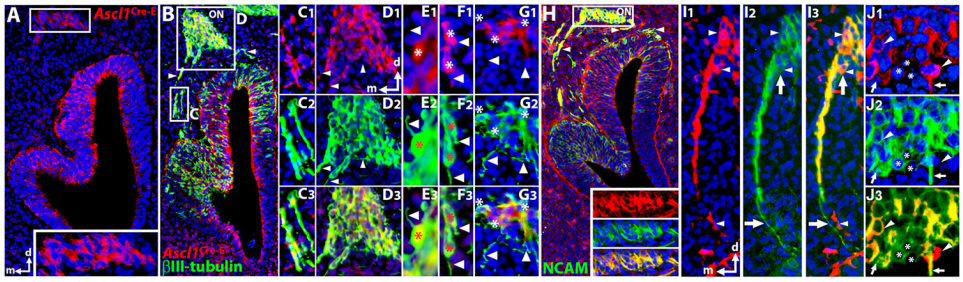

Figure 4:

Ascl1$^{Cre\text{-}E}$+ cells are associated with the developing olfactory nerve (ON) and migratory mass. **A**) *Ascl1*$^{Cre\text{-}E}$+are seen concentrated in the medial OE and in subset of frontonasal mesenchymal (fnm) cells (box and *inset*) that are morphologically and cytologically reminiscent of the cells of the migratory mass that forms in parallel with the initial outgrowth of the axons of early generated ORNs. *Ascl1*$^{Cre\text{-}E}$+ cells are not seen in other regions of the fnm. **B**) The distribution of βIII-tubulin+ cells as well as their processes in the OE and fnm and their relationship to *Ascl1*$^{Cre\text{-}E}$+ cells. βIII-tubulin+ cell frequency declines in the OE region where Ascl1Cre-E+ cells are concentrated. βIII-tubulin+ cells and process coalesce in the fnm to form fasciles (arrowheads, box **C**), as well as aggregating in the migratory mass to contribute to the nascent ON (box **D**) **C$_{1\text{-}3}$**) *Ascl1*$^{Cre\text{-}E}$+ cells (**C$_1$**) are in register with more extensively labeled βIII-tubulin+ axon fascicles (**C$_2$**) that extend from the OE toward the migratory mass and ON. The registration is not complete (yellow label indicates overlap, **C$_3$**). **D$^{1\text{-}3}$**) The perinuclear cytoplasm of migratory mass cells is labeled to identify apparent *Ascl1*$^{Cre\text{-}E}$+ migratory mass cells (**D$_1$**). βIII-tubulin+ cells and processes coincide with the *Ascl1*$^{Cre\text{-}E}$+ cells, but are not completely in register (compare arrowheads in **D$_{1,2}$**). **E$_{1\text{-}3}$, F$_{1\text{-}3}$**) Single *Ascl1*$^{Cre\text{-}E}$+ cell bodies (asterisk, **E$_1$**, **F$_1$**) are also labeled for βIII-tubulin (red asterisks, **E$_{2,3}$**; **F$_{2\text{-}3}$**). These cells have leading or trailing processes (arrowheads) that are labeled for βIII-tubulin (**E$_{2,3}$**; **F$_{2\text{-}3}$**) but not *Ascl1*$^{Cre\text{-}E}$. **G$_{1\text{-}3}$**) Aggregates of *Ascl1*$^{Cre\text{-}E}$+ cell bodies (**G$_1$**, asterisks) are adjacent to apparent small fascicles or single βIII-tubulin+ axons (arrowheads, **G$_{2,3}$**) that appear to coalesce into a larger fascicle as they reach the aggregated *Ascl1*$^{Cre\text{-}E}$+ cells. **H**) NCAM labels a subset of dorsolateral and ventromedial OE cells, including a sub-population of presumed ORNs that are actively extending axons into the fnm toward the nascent ON. NCAM also labels the *Ascl1*$^{Cre\text{-}E}$+ cells associated with the migratory mass. The lack of a significant number of *Ascl1*$^{Cre\text{-}E}$+ presumed ORNs makes it highly unlikely that the Ascl1Cre-E labeling is due to axons rather than labeling of the perinuclear cytoplasm of Ascl1Cre-E+ cells in the fnm, including those in the migratory mass (box and *inset*). **I$_{1\text{-}3}$**) A fascicle of NCAM+ axons, including either a small fascicle or single NCAM+ axon (large arrowhead, **I$_1$**) and some NCAM+ fnm cells (small arrowhead) appear to coalesce in the fnm where they coincide with, but do not totally overlap a chain of *Ascl1*$^{Cre\text{-}E}$+ fnm cells (**I$_2$**) that aggregate in register with the NCAM+ axons (arrows, **I$_{1\text{-}3}$**) to join the nascent ON. **J**) In some migratory mass aggregates, there are subsets of *Ascl1*$^{Cre\text{-}E}$+ fnm cells (**J$_1$**, arrowheads) that are intercalated with larger apparent NCAM+ axon fascicles (arrows, **J$_{1\text{-}3}$**) as well as NCAM +/*Ascl1*$^{Cre\text{-}E}$– presumed migratory mass cells (asterisks).

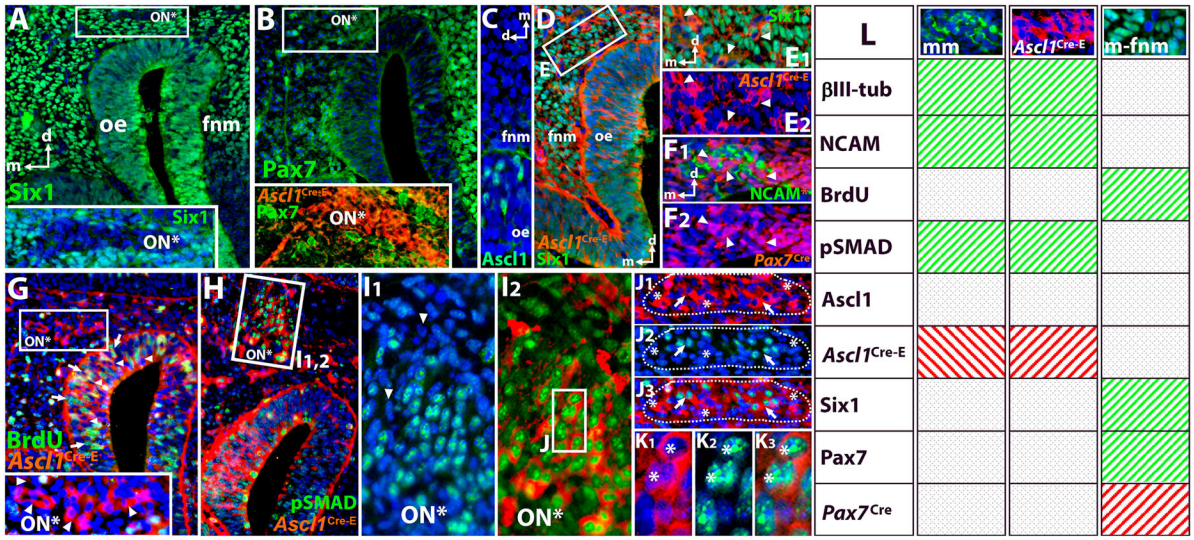

Figure 5:

Distinctions in identity and lineage of ON-associated frontonasal mesenchyme (fnm) cells. **A**) Six1+ fnm cells are concentrated in the medial and dorsolateral fnm, but attenuated in the lateral ventral fnm. In the dorsomedial fnm however, there are regions where Six1+cells are not seen (box and *inset*), presumably where the olfactory nerve (ON*) are found. **B**) Pax7+ (protein) cells are concentrated in the lateral fnm. In the mediodorsal fnm where fascicles of the olfactory nerve are presumably growing (ON*) there are few, if any Pax7+ cells. In this mediodorsal region where Pax7+ cells are absent, *Ascl1*$^{Cre\text{-}E}$+ cells accumulate (box, *inset*, ON*). **C**) Cells in the fnm adjacent to the OE region where Ascl1+ (protein) cells are found do not express Ascl1. **D**) Six1+ cells predominate in the medial fnm. There are, however, a small population of *Ascl1*$^{Cre\text{-}E}$+/Six1− cells that accumulate in the fnm region where the olfactory nerve is seen. **F$_{1\text{-}2}$**) NCAM+ axons and cells of the nascent olfactory nerve (ON; **C$_1$**) and migratory mass are seen at the boundary of the medial and lateral fnm, distinct from a subset of *Pax7*^{Cre}+ cells (arrowheads **F$_{1,2}$**). **G**) *Ascl1*$^{Cre\text{-}E}$+ cells in the medial fnm are not acutely labeled by BrdU, in contrast to *Ascl1*$^{Cre\text{-}E}$+ (arrows) or *Ascl1*$^{Cre\text{-}E}$ – (arrowheads)cells in the OE as well as a subset of *Ascl1*$^{Cre\text{-}E}$– cells in the fnm. **H**) *Ascl1*$^{Cre\text{-}E}$+ cells in the presumed olfactory nerve (ON*) and migratory mass (box; enlarged in **H$_{1,2}$**), as well as in the dorsomedial OE (arrows), are also pSMAD+. These cells are segregated within the fnm in the region where the olfactory nerve (ON*) typically coalesces as it extends toward the ventral forebrain. **H$_{1\text{-}2}$**) pSMAD+ cells define a restricted fnm subpopulation. pSMAD+ nuclei (**H$_1$**) tend to be aligned in the region of the presumptive olfactory nerve (ON*) and migratory mass; however, there are also pSMAD- cells in this region (arrowheads). Many pSMAD+ fnm cells in the region of the presumptive ON are also *Ascl1*$^{Cre\text{-}E}$+. **J$_{1\text{-}3}$**) An accumulation of *Ascl1*$^{Cre\text{-}E}$+ cells with pSMAD- nuclei (asterisks) and *Ascl1*$^{Cre\text{-}E}$+ cells with pSMAD+ nuclei (arrows) define a limited region of the fnm that presumably corresponds to the coalescing ON (dotted outline). **K$_{1\text{-}3}$**) Nuclei of *Ascl1*$^{Cre\text{-}E}$+ cells in this region are pSMAD+ (asterisks). **L**) Molecular and proliferative marker profiles of migratory mass (mm; NCAM+ cells shown), medial fnm *Ascl1*$^{Cre\text{-}E}$+ cells, and medial fnm cells (m-fnm). The profiles of migratory mass and medial fnm *Ascl1*$^{Cre\text{-}E}$+ cells are

identical. Diagonal, colored hatching indicates labeling for the relevant marker, dotted shading indicates lack of labeling.

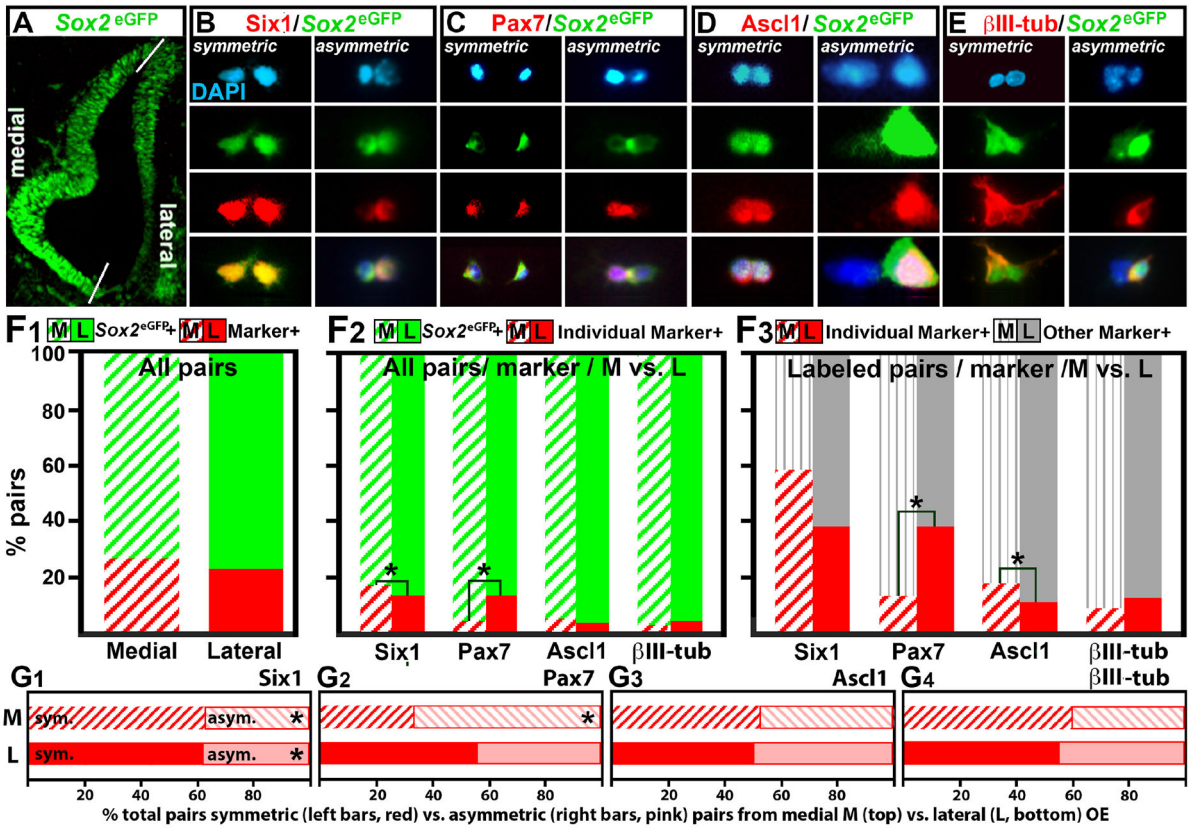

Figure 6:

Molecular identity and OE medial versus lateral position influence modes of precursor proliferation and division. **A**) A *Sox2*^{eGFP} reporter transgene labels lateral and medial OE cells in a graded fashion. Symmetric and asymmetric divisions of **B**) Six1+/*Sox2*^{eGFP}+ precursor cell pairs recorded and scored in this analysis; **C**) Pax7+/*Sox2*^{eGFP}+ cell pairs; **D**) Ascl1+/*Sox2*^{eGFP}+ cell pairs. **E**) Symmetric and asymmetric neurogenic divisions from *Sox2*^{eGFP}+ progenitors identified with βIII-tubulin. **F**) Normalized frequency of medial versus lateral cell pairs. **F$_1$**) The frequency of medial versus lateral pairs labeled by *Sox2*^{eGFP} and any of the four additional markers does not differ significantly. **F$_2$**) The frequencies of Six1+ and Pax7+ pairs as a proportion of all *Sox2*^{eGFP}+ medial versus lateral cell pairs differ significantly (asterisks, Six1+ M > Six1+ L, $p \leq 0.04$; Fisher-Exact; Pax7+ M < Pax7+ L, $p \leq 0.001$, Fisher-Exact). **F$_3$**) Pax7+ pairs are significantly more frequent among lateral pairs (asterisk. $p \leq 0.0001$; Fisher-Exact) and Ascl1+ pairs are more frequent among medial pairs (asterisk, $p \leq 0.03$, Fisher-Exact) when frequency of medial versus lateral pairs is compared for each marker class as a proportion of all medial or lateral *Sox2*^{eGFP}+ pairs labeled for any of the four markers. **G**) Normalized frequency of symmetric versus asymmetric dividing cell pairs from the medial and lateral OE. **G$_1$**) For medial and lateral Six1+ pairs, there are significantly more symmetric divisions ($p \leq 0.0001$ medial; 0.03, lateral; Fisher Exact). **G$_2$**) There are significantly fewer symmetric divisions among lateral Pax7+ pairs ($p \leq 0.03$, Fisher Exact); however, the frequency of symmetric versus asymmetric divisions for medial Pax7+ cell pairs do not differ significantly. **G$_3$**) There is no significant difference in symmetric versus asymmetric divisions for medial or lateral Ascl1+

pairs. **G_4**) There is no significant difference in neurogenic symmetric versus asymmetric divisions (βIII-tubulin+) for medial or lateral pairs.

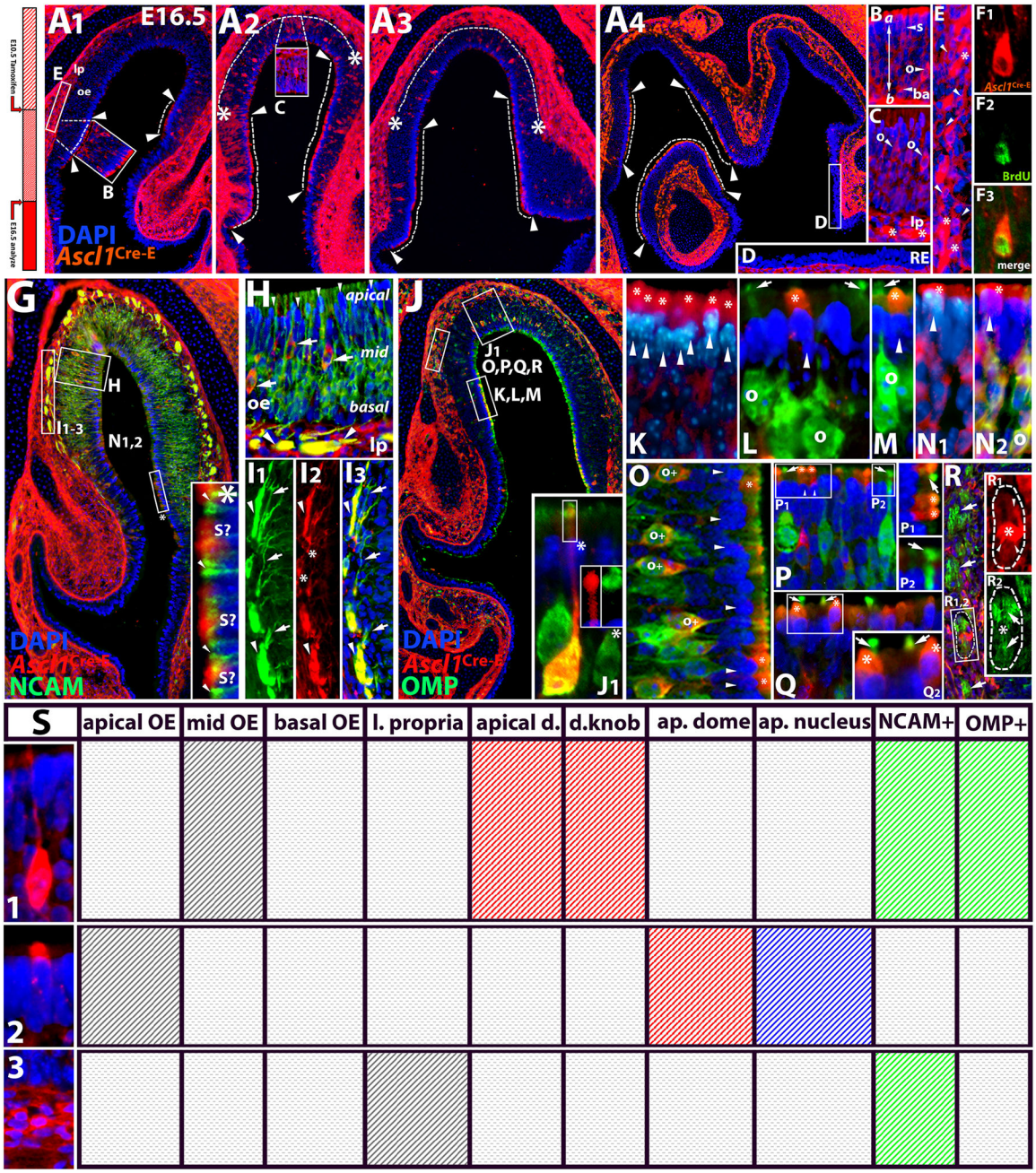

Figure 7:

Distribution and identities of E10.5 recombined (E10.5-R) *Ascl1*$^{\text{Cre-E}}$+ precursor cohort in the E16.5 OE. **A$_{1\text{-}4}$**) Series of sections showing the distribution of E10.5-R *Ascl1*$^{\text{Cre-E}}$+ cells in the E16.5 OE. The dotted lines between arrowheads indicate regions where apparent sustentacular/supporting cells and their processes predominate, primarily in the more ventral aspect of the anterior OE at the transition from apparent respiratory epithelium. The dotted lines between asterisks indicate regions where apparent E10.5-R *Ascl1*$^{\text{Cre-E}}$+ ORNs predominate, primarily in dorsal anterior OE regions. The areas boxed in A1-4 are enlarged in **B-E**. **B**) A region where E10.5-R *Ascl1*$^{\text{Cre-E}}$+ apparent sustentacular/supporting cells (s,

arrowhead), based upon their morphology (see also panel **G**, inset; panels **K-M** & **K_1-M_1**), are most frequent. Many *Ascl1*$^{Cre\text{-}E}$+ apparent sustentacular cells have apical extensions that end in club-like processes at the apical (*a*)/lumenal surface. Other E10.5-R *Ascl1*$^{Cre\text{-}E}$+ cells are seen at more basal positions (*b*). **C**) A region where apparent *Ascl1*$^{Cre\text{-}E}$+ ORNs (arrowheads), based upon their morphology including dendrites that extend toward the apical/lumenal surface, predominate. In the lamina propria (lp) reporter labeling (asterisks) likely reflects ORN axon fascicles and/or ensheathing cell processes that coalesce after the axons exit the OE. **D**) There are no E10.5-R *Ascl1*$^{Cre\text{-}E}$+ cells in the apparent respiratory epithelium (RE). **E**) In the lamina propria distal to the OE, E10.5-R *Ascl1*$^{Cre\text{-}E}$+ cells and processes accumulate. E10.5-R *Ascl1*$^{Cre\text{-}E}$+ cells (arrowheads), including some that are adjacent to apparent accumulations of processes (asterisks) that may comprise ORN axons as well as processes of E10.5-R *Ascl1*$^{Cre\text{-}E}$+ cells in the lamina propria. **F**) After chronic BrdU exposure from E11.5 through 13.5 via maternal drinking water, BrdU+ nuclei are E10.5-R *Ascl1*$^{Cre\text{-}E}$ + cells (**F_1**) very rarely have nuclei heavily labeled for BrdU (**$F_{2,3}$**). **G-I**) Infrequent E10.5-R *Ascl1*$^{Cre\text{-}E}$+ cells (box, **H**) whose morphology suggests that they are ORNs are seen among the far more numerous NCAM+ presumptive ORNs. In addition, E10.5-R *Ascl1*$^{Cre\text{-}E}$ apical processes (box, *) that resemble the apical domains of OE sustentacular/supporting cells (inset, S?) are interdigitated between NCAM+ apical dendrites and dendritic knobs (inset, arrowheads). **H**) E10.5-R *Ascl1*$^{Cre\text{-}E}$+ cell bodies (arrows) are NCAM− and are surrounded by NCAM+ apparent ORN cell bodies in the mid-level of the OE. A palisade of heavily labeled DAPI+ nuclei (arrowheads) is seen in the apical OE. In the lamina propria (lp), E10.5-R *Ascl1*$^{Cre\text{-}E}$+ cells and processes appear to coincide with NCAM+ ORN axon fascicles (arrowheads). **$I_{1\text{-}3}$**) Small fascicles or individual NCAM+ axons (arrows) exit the OE, extend through the lamina propria and coalesce adjacent to, or overlapping, E10.5-R *Ascl1*$^{Cre\text{-}E}$+ cells (asterisks) and processes (arrowheads) that are both NCAM+ and NCAM−. **J**) E10.5-R *Ascl1*$^{Cre\text{-}E}$+ cells are found among OMP+ ORNs in the E16.5 dorsal anterior OE. **J_1**) Occasional *Ascl1*$^{Cre\text{-}E}$+ ORNs are also OMP+. Dual labeling extends to their apical dendrites and dendritic knobs (*inset*, *). **K**) *Ascl1*$^{Cre\text{-}E}$+ cells include a population whose nuclei are aligned at the apical aspect of the OE (arrowheads) and whose apical domains have a dome or club-like morphology (asterisks). **L**) Cytological and positional distinction between an *Ascl1*$^{Cre\text{-}E}$+ cell with an apical nucleus (arrowhead) and a dome-shaped apical domain (asterisk) and OMP+ ORNs (o) in the mid-level of the OE whose apical dendrites and dendritic knobs (arrows) also extend to through the apical OE and into the OE lumen. **M**) An OMP+ dendritic knob (arrow) from an OMP+ ORN (o) with its cell body in the mid-OE **$N_{1,2}$**) *Ascl1*$^{Cre\text{-}E}$+ cells with apically positioned nuclei (example indicated with arrowhead) and an apical/lumenal dome-shaped domain (asterisk) are distinct from NCAM+ cell bodies in the mid-OE. (o) that are actively extending an axon toward the OB. **O, $P_{1,2}$**) Subsets of OMP+ ORN cell bodies are also *Ascl1*$^{Cre\text{-}E}$+ (o+), amid OMP+/*Ascl1*$^{Cre\text{-}E}$-ORNs in the mid-OE. These cells and their apically directed processes are distinct from the dome-shaped *Ascl1*$^{Cre\text{-}E}$+ cells whose heavily labeled DAPI+ nuclei form a palisade in the apical OE (arrowheads). OMP+/*Ascl1*$^{Cre\text{-}E}$− ORN apical dendrites and dendritic knobs (arrows, **P_1**, **P_2**) are distinct from *Asc1*$^{Cre\text{-}E}$+/OMP− cells with apically localized nuclei and dome-shaped apical domains (arrowheads, asterisks, **P_1**). **$Q_{1,2}$**) *Ascl1*$^{Cre\text{-}E}$+ cells with apically localized nuclei and dome-shaped apical domains (asterisks, **$Q_{1,2}$**) are adjacent to OMP+ labeled dendritic knobs (arrows, **$Q_{1,2}$**). **$R_{1,2}$**) In the lamina

propria adjacent to regions where OMP+ ORNs as well as *Ascl1*$^{\text{Cre-E}}$+ ORNs are found, there are accumulations of OMP+ axon fascicles (dotted lines, arrows, **R$_{1,2}$**), some of which have associated with them *Ascl1*$^{\text{Cre-E}}$+ cells with multiple processes (asterisk, arrowheads, **R$_{1,2}$**). **S**) Three classes of E10.5-R *Ascl1*$^{\text{Cre-E}}$+ cells (left) are seen in the E16.5 OE and adjacent lamina propria. Class 1 cells have cell bodies in the mid-OE, apically oriented dendrites, and dendritic knobs. They are found among NCAM+ presumed ORNs and a subset of these *Ascl1*$^{\text{Cre-E}}$+ cells express OMP. Class 2 cells are found in the apical OE, have heavily labeled DAPI+ nuclei, apical domes, and do not express NCAM or OMP. Class 3 cells are found in the lamina propria, some express NCAM, but none express OMP. Diagonal colored hatching indicates *Ascl1*$^{\text{Cre-E}}$ (red), DAPI (blue) or NCAM/OMP labeling; black diagonal hatching indicates OE/lamina propria position for each cell class, and dashed shading indicates properties that each class does not have.

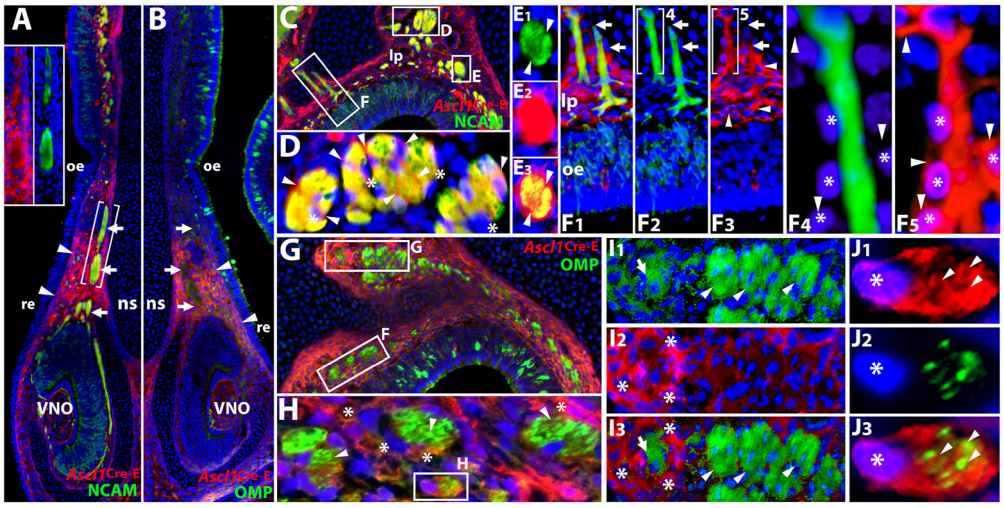

Figure 8:

E10.5- *Ascl1*$^{\text{Cre-E}}$ + cells envelop distinct classes of ORN axons in the lamina propria and coalescing olfactory nerve at E16.5. **A, B**) *Ascl1*$^{\text{Cre-E}}$+ cells intercalated between the OE, the nasal septum (ns), the vomeronasal organ (vno), the respiratory epithelium (re) and the olfactory epithelium (oe). These cells surround fascicles of NCAM+ axons presumable from NCAM+ VNO receptor neurons (**A**, brackets, *inset*) as well as apparent fascicles that include a small population of presumed OMP+ axons from (**B**). **C**) Fascicles of NCAM+ axons coalesce in the lamina propria (lp) dorsally (boxes, panels **D**, **E**, **F**). **D**) Some fascicles have multiple NCAM+ bundles bounded by septae (arrowheads) of presumed E10.5-R *Ascl1*$^{\text{Cre-E}}$+ ensheathing cells whose DAPI+ nuclei are also seen within and at the margin of these fascicles (asterisks). **E$_{1\text{-}3}$**) NCAM+ axons gathered into a single multi-domain bundle in the lamina propria are surrounded by DAPI+ nuclei (**E$_1$**) in region where fewer axons are seen (arrowheads). The DAPI+ nuclei belong to E10.5-R *Ascl1*$^{\text{Cre-E}}$+ cells (**E$_2$**) whose processes fill the entire where the NCAM+ axon fascicles are seen. These processes (**E$_3$**) make septa (arrowheads) that divide the bundle of NCAM+ axons into smaller fascicles. **F$_{1\text{-}5}$**) Linear fascicles of NCAM+ ORN axons (**F$_1$**; bracket, arrows, **F$_2$**) extend through a more broadly distributed population of E10.5-R *Ascl1*$^{\text{Cre-E}}$+ cells with DAPI+ nuclei and processes (arrowheads, **F$_3$**). E10.5-R *Ascl1*$^{\text{Cre-E}}$+ cells that are not NCAM+ (asterisks, **F$_{4,5}$**) have processes (arrowheads, **F$_{4,5}$**) that are coincident with NCAM+ axon fascicles. **G**) OMP+ E10.5-R *Ascl1*$^{\text{Cre-E}}$– ORN axons constitute subsets of larger ON fascicles that are bounded by E10.5-R *Ascl1*$^{\text{Cre-E}}$+ cells and processes. **H**) Multiple OMP+ ORN axon fascicles (arrowheads) surrounded by E10.5-R *Ascl1*$^{\text{Cre-E}}$+ cells and processes (asterisks). **I$_{1\text{-}3}$**) Multiple OMP+ ORN axon fascicles (arrowheads, **I$_{1,3}$**) do not have adjacent enveloping E10.5-R *Ascl1*$^{\text{Cre-E}}$+ cells. In contrast, some OMP+ ORN axon fascicles (arrow, **I$_{1,3}$**) are surrounded by an aggregate of E10.5-R *Ascl1*$^{\text{Cre-E}}$+ cells (asterisks, **I$_{2,3}$**). **J$_{1\text{-}3}$**) A single E10.5-R *Ascl1*$^{\text{Cre-E}}$+ cell (**J$_1$**) with a DAPI+ nucleus (left, asterisk) has a single lamellate fenestrated process (arrowheads, **J$_1$**) that envelops multiple small OMP+ ORN axon fascicles (**J$_2$,** arrowheads, **J$_3$**).

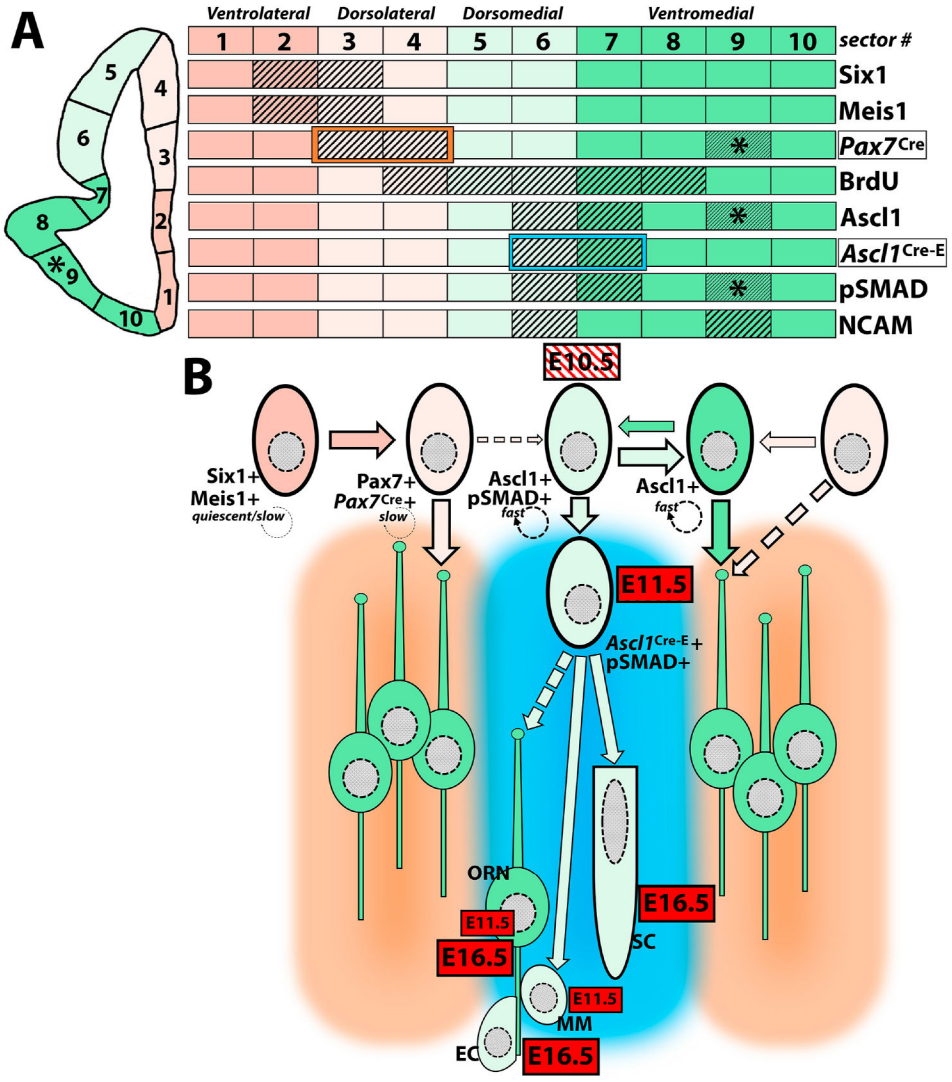

Figure 9:

Temporal, molecular and regional and distinctions between OE precursors suggest at least two primarily independent early OE lineages. **A**) A summary of focal regional expression of transcription factors expressing distinct markers with regional differences in cell proliferation, molecular correlates of signal transduction, and differentiated neurons at the onset of OE differentiation (E11.5). The hatched lines indicate sectors where the two highest frequencies of each cell class are recorded (see Figures 1, 2 and 3). There is also a fairly distinct population of cells in the ventromedial OE that express Pax7, are labeled by *Pax7*^{Cre} recombination, express Ascl1 protein, and have enhanced frequency of pSMAD+ nuclei (see Figure 1, 2; finer hatching and asterisks). Transcriptionally fate-mapped populations characterized here, *Pax7*^{Cre}+and *Ascl1*$^{Cre\text{-}E}$+ cells are largely segregated (dark salmon and teal boxes), suggesting they reflect two mostly independent lineages derived from distinct regions of the early differentiating OE. **B)** A proposed schematic of precursor identity and progression for early populations of lateral (dark and lite salmon) and medial (light and dark green) OE precursors. Early precursors that are primarily Six+/Meis1+ are most likely to be

found in the ventrolateral OE (dark salmon) and either quiescent or minimally proliferative (slow). These precursors generate Pax7+ progeny (light salmon, middle left) and divide slowly to yield initial ORN cohorts o, primarily in the dorsomedial and ventromedial OE (salmon shading, left). Some of these cells may yield a small number of Ascl1+ dorsolateral precursors (light salmon, dotted arrow, right); however, our data does not suggest that these precursors generate appreciable numbers of *Pax7*^{Cre}+/Ascl1+ progeny. A second population of Ascl1+ medial precursors occupy the lower dorsomedial and upper ventromedial OE. They are more proliferative ("fast", reflecting higher BrdU+ cell frequency), more likely to be pSMAD+, and appear to give rise to a spatially restricted population of Ascl1-derived OE *Ascl1*$^{Cre\text{-}E}$+ precursors that generate a minimal ORNs as well as more frequent apparent migratory mass cells (MM) by E11.5, and then a subset of ORNs, apparent sustentacular (SC) and ensheathing cells (EC) identified based upon a matrix comparison of OE position and marker expression (see Figure 7) at E16.5 (teal; center). Finally, a small population of Pax7+/Ascl1+ precursors in the extreme ventromedial OE (far right, smaller hatching) may generate additional early ORNs (salmon shading, right) in an OE region of the that will presumably contribute to the VNO.